HHS Public Access

Author manuscript

Sci Transl Med. Author manuscript; available in PMC 2023 January 03.

Published in final edited form as:

Sci Transl Med. 2022 November 02; 14(669): eabo1981. doi:10.1126/scitranslmed.abo1981.

Hormonal Therapies Upregulate MANF and Overcome Female Susceptibility to Immune Checkpoint Inhibitor-Myocarditis

Yaohua Zhang[1,2,#,*], **Chengcao Sun**[1,#], **Yajuan Li**[1,3,#], **Juan Qin**[4,#], **Kaushik Amancherla**[5], **Ying Jing**[6], **Qingsong Hu**[1,7], **Ke Liang**[1], **Zhao Zhang**[6], **Youqiong Ye**[6], **Lisa A. Huang**[1], **Tina K. Nguyen**[1], **Sergey D. Egranov**[1], **Zilong Zhao**[1], **Andrew Wu**[1], **Yutao Xi**[8], **Jun Yao**[1], **Mien-Chie Hung**[9,10], **George A. Calin**[11,12], **Jie Cheng**[8], **Bora Lim**[13], **Lorenz H. Lehmann**[14], **Joe-Elie Salem**[15], **Douglas B. Johnson**[16], **Michael A. Curran**[17], **Dihua Yu**[1,18], **Leng Han**[19], **Radbod Darabi**[20], **Liuqing Yang**[1,12,18,*], **Javid J. Moslehi**[4,*], **Chunru Lin**[1,18,*]

[1]Department of Molecular and Cellular Oncology, The University of Texas MD Anderson Cancer Center, Houston, TX, 77030, USA.

[2]Beijing Institute of Brain Disorders, Collaborative Innovation Center for Brain Disorders, Capital Medical University, Beijing, 10069, China.

[3]Current address: Incyte Corporation, Wilmington, DE 19803, USA

[4]Section of Cardio-Oncology & Immunology, Division of Cardiology and the Cardiovascular Research Institute, University of California San Francisco, San Francisco, CA, 94143, USA

[5]Department of Medicine, Vanderbilt University of Medical Center, Nashville, TN 37232

[6]Department of Biochemistry and Molecular Biology, The University of Texas Health Science Center at Houston McGovern Medical School, Houston, TX 77030, USA

[7]Current address: The First Affiliated Hospital of USTC, Division of Life Sciences and Medicine, University of Science and Technology of China, Hefei, Anhui, 230001, P.R. China.

[8]Texas Heart Institute, St. Luke's Hospital, Houston, TX 77030, USA.

[9]Graduate Institute of Biomedical Sciences, Research Center for Cancer Biology, and Center for Molecular Medicine, China Medical University, Taichung 404, Taiwan.

[10]Department of Biotechnology, Asia University, Taichung 413, Taiwan.

[*]Corresponding author. YZhang57@mdanderson.org (Y.Z.); lyang7@mdanderson.org (L.Y.); Javid.Moslehi@ucsf.edu (J.J.M.); and clin2@mdanderson.org (C.L.).

[#]Denotes equal contribution

Author contributions: Conceptualization: J.J.M., L.Q.Y. and C.R.L.; Methodology: Y.H.Z., J.Q., C.C.S., D.B.J., K.A., Y.J.L., Q.S.H., T.K.N., K.L., L.A.H., Z.L.Z., Y.X., and J.C.; Bioinformatic analysis: J.Y., Z.Z., Y.Q.Y., Y.J. and L.H.; Editorial comments: B.L., L.H.L., J.E.S., D.H.Y., M.C.H., G.A.C., M.A.C., and R.D.; Writing – original draft: C.R.L. Y.H.Z. A.W. and S.D.E.; Writing – review & editing: J.J.M., C.R.L., Y.H.Z., A.W.

Competing interests: Authors declare that they have no competing interests. JJM has served on advisory boards for Bristol-Myers Squibb, Takeda, AstraZeneca, Myovant, Kurome Therapeutics, Star Therapeutics, and Cytokinetics.

Supplementary Materials
Materials and Methods
Figs. S1 to S15
Tables S1 to S4
Data file S1
References (67–75)
MDAR Reproducibility Checklist

[11]Department of Experimental Therapeutics, Division of Cancer Medicine, The University of Texas MD Anderson Cancer Center, Houston, TX, 77030, USA.

[12]Center for RNA Interference and Non-Coding RNAs, The University of Texas MD Anderson Cancer Center, Houston, TX, 77030, USA.

[13]Department of Breast Medical Oncology, The University of Texas MD Anderson Cancer Center, Houston, TX 77030, USA.

[14]Department of Cardiology, Heidelberg University Hospital, Heidelberg, Germany; Cardio-Oncology Unit, Heidelberg University Hospital, Heidelberg, Germany; German Cardiovascular Research Center (DZHK), partner site Heidelberg/Mannheim, Germany; German Cancer Research Center (DKFZ), Heidelberg, Germany

[15]Deprtment of Pharmacology, Assistance Publique-Hôpitaux de Paris (AP-HP), Sorbonne Université, INSERM, CIC-1901, UNICO-GRECO Cardiooncology Program, Paris, France.

[16]Vanderbilt-Ingram Cancer Center, Vanderbilt University Medical Center, Nashville, TN, 37232, USA

[17]Department of Immunology and Scientific Director of the Oncology Research for Biologics and Immunotherapy Translation (ORBIT), The University of Texas MD Anderson Cancer Center, Houston, TX 77030, USA.

[18]The Graduate School of Biomedical Sciences, The University of Texas MD Anderson Cancer Center, Houston, TX, 77030, USA.

[19]Center for Epigenetics and Disease Prevention, Institute of Biosciences and Technology, Texas A&M University, Houston, TX, 77030, USA.

[20]Center for Stem Cell and Regenerative Medicine (CSCRM), The Brown Foundation Institute of Molecular Medicine for the Prevention of Human Diseases (IMM), The University of Texas Health Science Center at Houston, Houston, TX, 77030, USA.

Abstract

Immune checkpoint inhibitors (ICIs) have been increasingly used in combination for cancer treatment but are associated with myocarditis. Here, we report that tumor-bearing mice exhibited response to treatment with combinatorial anti-PD-1 (programmed cell death 1) and anti-CTLA-4 (Cytotoxic T-lymphocyte Antigen-4) antibodies but also presented with cardiovascular toxicities observed clinically with ICI therapy, including myocarditis and arrhythmia. Female mice were preferentially affected with myocarditis compared to male mice, consistent with a previously described genetic model of ICI-myocarditis as well as emerging clinical data. Mechanistically, myocardial tissue from ICI-treated mice, the genetic mouse model, and human heart tissue from affected patients with ICI-myocarditis all exhibited downregulation of *MANF* (Mesencephalic Astrocyte Derived Neurotrophic Factor) and *HSPA5* (Heat Shock 70kDa Protein 5) in the heart; this downregulation was particularly striking in female mice. ICI-myocarditis was amplified by heart-specific genetic deletion of mouse *Manf* and was attenuated by administration of recombinant MANF protein, suggesting a causal role. Ironically, both *MANF* and *HSPA5* were transcriptionally induced by liganded estrogen receptor-βbeta and inhibited by androgen receptor. However, ICI treatment reduced serum estradiol concentration to a greater extent in female

compared to male mice. Treatment with an estrogen receptor β-specific agonist as well as androgen depletion therapy attenuated ICI-associated cardiac effects. Taken together, our data suggest that ICI treatment inhibits estradiol-dependent expression of *MANF/HSPA5* in the heart, curtailing the cardiomyocyte response to immune injury. This endocrine-cardiac-immune pathway offers new insights into the mechanisms of sex differences in cardiac disease and may offer treatment strategies for ICI-myocarditis.

One Sentence Summary:

ICI inhibits estradiol-induced cardiac *MANF/HSPA5* expression, leading to myocarditis that could be attenuated by recombinant MANF or hormone therapy.

INTRODUCTION

Immune checkpoint inhibitors (ICIs) have advanced options for nearly 50% of cancer patients (1–3). PD-1, PD-L1, and CTLA-4 are the most comprehensively characterized antibody-mediated targets of several successful drug therapies(4–7). ICIs are used in combination (for example, anti-PD-1 and anti-CTLA4) (8, 9), which results in enhanced anti-tumor efficacy, but a broad spectrum of immune-related adverse events (irAE) can occur(9, 10). Cardiovascular toxicities including myocarditis, are most problematic and result increased mortality(11–13). ICI-associated myocarditis is characterized by electrocardiographic abnormalities, particularly atrial fibrillation, and conduction disease, with systolic cardiac function occurring in about half of patients (14, 15). Endomyocardial biopsy, characterized by patchy inflammatory infiltrates and cardiomyocyte death, is the most definitive means of ICI-myocarditis diagnosis (16). Several pre-clinical models of ICI-myocarditis have been generated to enhance our understanding of underlying pathophysiology (17–21). These include pharmacological models as well as a genetic model whereby monoallelic loss of *Ctla4* (encoding CTLA-4) in the context of complete genetic absence of *Pdcd1* (encoding PD-1) leads to myocardial immune infiltration and severe electrocardiographic abnormalities, recapitulating the ICI-associated myocarditis observed in patients (18). In all these models, myocardial tissues show predominantly $CD8^+$ T cells interspersed with $CD4^+$ T cells and macrophages (22). However, the underlying mechanisms of ICI-associated myocarditis, in particular contributions from genetic and environmental factors, remain largely elusive. Clinically, females are more susceptible to ICI-associated myocarditis independent of other clinical parameters (23, 24). In the genetic mouse model of ICI-myocarditis, female $Ctla4^{+/-}$ $Pdcd1^{-/-}$ mice have greater mortality and a more fulminant course compared to male $Ctla4^{+/-}$ $Pdcd1^{-/-}$ mice (18). The emerging clinical and pre-clinical data with ICI-myocarditis are intriguing because in non-ICI-myocarditis (viral or autoimmune), male sex is considered an important risk factor and associates with a more fulminant course (25), which suggests a possible interaction of immune checkpoints, sex hormones and the heart, perhaps providing insights into the mechanisms of sex-based differences in heart disease.

While immune dysregulation plays a critical role in inflammatory cardiomyopathies such as ICI-myocarditis, it is less clear what roles myocardial compensatory and protective processes play in attenuating immune infiltration. Heart-specific proteins, especially secreted

ones (“cardiokines”), have been identified in cardiac stress and injury models and include members of the transforming growth factor-β superfamily (e.g., Growth Differential Factors 15 and 8), Migration Inhibitory Factor (MIF), and endoplasmic reticulum (ER)-stress induced proteins (26–29). Cardiac intrinsic protective factors are important to explore in ICI-myocarditis, not just for scientific reasons but also for therapeutic purposes, since focusing on inhibiting the immune system may also dampen the anti-tumor effects of ICI and other immune-mediated therapies (13, 30).

Here, we developed a tumor-bearing, pharmacological model of ICI-associated myocarditis, replicating the clinical correlates in patients with ICI-myocarditis. In this model we concomitantly assessed tumor response following ICI treatment (anti-CTLA4 and anti-PD1 treatment). Using this pharmacological model, the genetic *Ctla4*$^{+/-}$ *Pdcd1*$^{-/-}$ mouse model and myocardial samples from patients with ICI-myocarditis, we studied underlying sex differences, specifically female predilection to ICI-myocarditis. Further, we explored cardiac-intrinsic responses that may play a role in regulating cardiac-immune interactions and tested whether targeting these factors would attenuate cardiac inflammation without disturbing anti-cancer effects of the ICI.

RESULTS

Immune checkpoint blockers induce cardiac complications

To investigate the mechanisms of ICI-associated myocarditis and other cardiovascular sequelae in cancer patients and to assess the interactions of tumors on these side-effects, we generated three mouse tumor models representing colorectal cancer (MC38) (31), melanoma (B16F10) (32), and breast cancer (EO771) (33) using both male and female C57BL/6J mice with tumor volumes reaching 200–250 mm^3 (Fig. 1A). Age- and gender-matched wild type C57BL/6J mice (WT) without tumor inoculation were included as controls (Fig. 1A). Both tumor-bearing and non-tumor-bearing mice were subjected to combination anti-PD-1 and anti-CTLA-4 antibody treatment, using doses that have been previously used to assess tumor efficacy. Combined anti-PD-1 and anti-CTLA-4 antibody treatment inhibited tumor growth and increased cleavage of caspase 3 and immune cell infiltration in the tumor upon ICI treatment (fig. S1). In addition, multiple tissues showed evidence of T cell infiltration (particularly $CD8^+$ T cells) including liver, kidneys, heart, skeletal muscle, and lung (fig. S1). ICI-associated irAEs were most physiologically problematic in the cardiovascular system. Affected mice exhibited myocarditis, electrocardiographic (ECG) disturbances, and mild cardiac systolic dysfunction. Histologically, mononuclear immune infiltration consisting of macrophages and $CD8^+$ T cells was observed in ICI-treated hearts but not in IgG-treated hearts, using CD8 and F4/80 as markers respectively (Fig. 1, B and C, and fig. S2, A to D). These cardiac findings were observed in both tumor-bearing and non-tumor-bearing mice post ICI treatment, suggesting minimal effects of tumor on the ICI-associated myocarditis (Fig. 1D and fig. S2, A and B). In addition, focal areas with myocardial dropout and areas with TUNEL-positive staining and cleaved-caspase 3 were observed (fig. S2, E to H). These results are consistent with several other pre-clinical models of ICI-myocarditis and clinical forms of ICI-myocarditis observed in patients.

ICI-associated myocardial effects were preferentially observed in female mice compared to male mice. ICI-treated female hearts exhibited increased $CD8^+$ T cell infiltration (Fig. 1D), electrocardiographic abnormalities (Fig. 1, E and F, and fig. S3, A to C), as well as depressed cardiac systolic dysfunction on echocardiography compared to male mice (fig. S3, D to J). These effects were not observed in either female or male isotype controls (Fig. 1F and fig. S3, D to J). Furthermore, mice treated with anti-PD-1, anti-CTLA-4 antibodies alone or in combination exhibited reduced ejection fraction and fractional shortening (fig. S3, K and L). To further ensure that the sex differences observed were not limited to our model of myocarditis, we assessed the recently described genetic model whereby *Ctla4*$^{+/-}$ *Pdcd1*$^{-/-}$ mice exhibited immune infiltration limited to the heart and led to a more fulminant form of myocarditis, characterized by premature mortality in affected mice (Fig. 1G). In this model, *Ctla4*$^{+/-}$ *Pdcd1*$^{-/-}$ female mice had a more fulminant course compared to *Ctla4*$^{+/-}$ *Pdcd1*$^{-/-}$ male mice (Fig. 1G). Both *Ctla4*$^{+/-}$ *Pdcd1*$^{-/-}$ mice and ICI-treated mice exhibited elevated serum Troponin I concentrations (fig. S3, M and N). Finally, recent data suggest that the serum levels of mmu-miR-721 are elevated in acute myocarditis, making this a more specific marker of myocarditis (vs. other cardiac injury such as ischemia) (34). *Ctla4*$^{+/-}$ *Pdcd1*$^{-/-}$ mice have elevated serum miR-721 levels in comparison to *Ctla4*$^{+/+}$ *Pdcd1*$^{+/+}$ female littermates (fig. S3O). The sex differences in ICI-myocarditis among patients have been harder to analyze given the increased proportion of male patients treated with ICI in clinical trials. However, the sex imbalance in our mice is consistent with emerging clinical data from patients where irAEs and myocarditis are more pronounced in females (23, 24). Taken together, our findings suggest that ICI-myocarditis preferentially manifests in female sex in multiple pre-clinical models, suggesting a possible connection between immune checkpoints, downstream immune or myocardial targets and sex hormones.

ICI modulates cardiac expression of MANF and HSPA5

To examine downstream affected pathways that are preferentially biased toward manifestation of myocarditis in female mice, we profiled the transcriptomes of the heart, kidneys, lungs, liver, and skeletal muscles following isotype IgG or ICI treatment (Fig. 2A, table S1, and **GSE145573**), focusing on differentially expressed genes (DEGs) in the heart (compared to other organs). Multiple genes and gene subsets were differentially expressed in the ICI-treated hearts compared to IgG-treated hearts including upregulation of gene set involved in reactive oxygen species (fig. S4A), suggesting that ICI treatment may impair the stress-response of cardiac muscles. Among heart-specific genes, Mesencephalic Astrocyte Derived Neurotrophic Factor (*Manf*) and Heat Shock 70kDa Protein 5 (*Hspa5*) transcription was decreased in expression upon ICI treatment in both the non-tumor-bearing and tumor-bearing hearts (Fig. 2B and fig. S4, B to E). Specifically, *Manf* downregulation was more pronounced in female hearts compared to male hearts post-ICI treatment (Fig. 2, C and D). Immunohistochemistry staining validated the downregulation of MANF and HSPA5 at the protein expression in the heart following ICI treatment (fig. S5, A to D), with confirmation by immunoblotting of a greater downregulation of MANF protein in female hearts compared to male hearts (fig. S5, E to G). To further expand these observations, we assessed *Manf* and *Hspa5* expression in the genetic ICI-myocarditis model. The cardiac expression of *Manf* was downregulated in *Ctla4*$^{+/-}$/*Pdcd1*$^{-/-}$ mice compared to *Ctla4*$^{+/+}$/*Pdcd1*$^{-/-}$ and *Ctla4*$^{+/+}$/*Pdcd1*$^{+/+}$ mice (fig. S6A). *Hspa5* expression was downregulated in both *Ctla4*$^{+/-}$/*Pdcd1*$^{-/-}$

and *Ctla4*$^{+/+}$/*Pdcd1*$^{-/-}$ compared to *Ctla4*$^{+/+}$/*Pdcd1*$^{+/+}$ mice (fig. S6B). Reduced MANF and HSPA5 protein expression negatively correlated with CD8^{+} staining intensity (Fig. 2E and fig. S6, C to H). Finally, MANF and HSPA5 protein expression were decreased in human heart tissues from patients with ICI-myocarditis compared to hearts of healthy donors (Fig. 2, F and G, and table S2). This downregulation was particularly striking in areas of more severe inflammation, correlating with elevated CD8^{+} T cell infiltration (fig. S6, I to L).

MANF is an evolutionary conserved protein related to unfolded protein response (UPR) with emerging data suggesting a protective role of MANF in ER stress-related diseases (35). While the role that MANF plays in the heart is only beginning to be explored, early data suggest that MANF is activated in cardiac ischemia and protects from cardiac injury via the UPR sensor and effector (35). HSPA5 (also known as ER chaperone BiP) has also been shown to be involved in protecting cardiomyocytes from injury (36). MANF directly interacts with HSPA5 in the ischemic heart (37). To assess whether MANF or HSPA5 plays regulatory roles in other forms of myocardial stress, we assessed the expression of *Manf* and *Hspa5* in an experimental myocardial ischemia model using permanent coronary artery ligation. *Manf* was upregulated 3 days following coronary artery ligation in wild-type mice, although the expression subsided 28 days following ligation (fig. S7). On the other hand, *Hspa5* was downregulated in the experimental myocardial ischemia model, both immediately after coronary ligation and later during cardiac remodeling (fig. S7). These findings contrast with our data in ICI-myocarditis where MANF, and possibly HSPA5, are both downregulated in mouse and human models. Collectively, our data suggest that *MANF* and *HSPA5* may regulate the interactions between the cardiovascular and immune systems during myocardial stress.

Depletion of *Manf* sensitizes hearts to ICI-associated myocarditis

To explore the functional role that *Manf* downregulation may play in myocardial homeostasis, we deleted *Manf* in adult mouse hearts by taking advantage of adeno-associated virus (AAV9)-delivered, saCas9-mediated gene editing, whereby cardiac troponin (cTnT)-driven expression of *saCas9* leads to cardiac-specific expression post-AAV delivery (38) (Fig. 3A). 3 weeks following AAV delivery, we confirmed reduced MANF protein expression in mice administered with AAV9-*Manf*-sagRNAs compared to mice administered with AAV9-Scr-sagRNAs or saline (Fig. 3, B and C, and fig. S8A). We also confirmed that sa*Cas9* was expressed in the heart but marginally in other organs following administration (Fig. 3C and D, and fig. S8B). *Manf*-proficient and -deficient animals were further subjected to tumor inoculation and ICI treatment. Heart-specific depletion of *Manf* resulted in minimal effects on the tumor growth of B16F10 xenografts following IgG or ICI treatment (fig. S8C). While ICI-treatment led to increased CD8 staining in both *Manf*-proficient and deficient mice, this increase was pronounced in *Manf*-deficient mice (Fig. 3, E and F). Furthermore, *Manf*-deficient hearts exhibited increased electrocardiographic disturbances as well as decreased systolic cardiac functions following ICI treatment. (Fig. 3, G to J). Hence, our findings suggested the functional importance of MANF in ICI-associated myocarditis.

MANF administration improves heart function following ICI treatment

Conversely, we asked whether MANF might protect against ICI-associated myocarditis. MANF has been suggested to associate with HSPA5 to form a macromolecular complex (37). Considering the potential fast degradation of recombinant proteins in human serum, we attempted to deliver recombinant MANF and HSPA5 proteins in a 1:1 ratio to achieve stabilized rMANF tissue pharmacokinetics (PK) *in vivo*. We first determined MANF serum concentrations, finding that wild type non-tumor-bearing mice harbor about 4 ng MANF per ml of serum (fig. S9A). Hence, we injected ~40 ng (2 μg/kg) rMANF and ~156 μg rHSPA5 (7.8 μg/kg) per animal to achieve a 1:1 molar ratio. To determine the PK of rMANF and rHSPA5, the heart tissues of non-tumor-bearing mice administered recombinant MANF and HSPA5 (2 μg/kg and 7.8 μg/kg respectively, i.p., daily) were harvested for immunohistochemistry staining to determine the presence of His-tagged-rMANF or c-Myc-tagged-HSPA5 (Fig. 4, A and B, and fig. S9, B and C). Immunofluorescence staining of the anti-His tag exhibited overlap with the anti-MANF antibody, suggesting the presence of His-tagged rMANF in heart (Fig. 4A and fig. S9A). Similarly, immunofluorescence staining of the c-Myc tag antibody exhibited overlap with the anti-HSPA5 antibody, suggesting the presence of c-Myc-tagged rHSPA5 in heart (Fig. 4B and fig. S9C). Animals treated with rMANF or rHSPA5 exhibited no obvious pathology. Specifically, rMANF or rHSPA5 treatment did not affect serum markers of liver or kidney function (fig. S10, A to D).

We then determined whether rMANF co-administered with rHSPA5 can attenuate ICI-associated myocarditis. Female mice were pre-treated with rMANF+rHSPA5, followed by inoculation with B16F10 cells (Fig. 4C). When tumors reached 200–250 mm^3, the animals were treated with IgG or ICI as described above (Fig. 4C). ICI treatment inhibited the growth of B16F10 tumors; rMANF+rHSPA5 treatment had no effects on tumor growth nor did it affect the anti-tumor effects of ICI treatment (fig. S10E). Histologically, treatment with rMANF+rHSPA5 had no effects on tumor infiltrating $CD8^+$ T cells (fig. S10, F and G). However, treatment with rMANF+rHSPA5 attenuated macrophage and $CD8^+$ T cell infiltration in the heart, decreased arrhythmogenicity and conduction disease, and improved cardiac function as assessed through echocardiography (Fig. 4, D to J, and fig. S10, H and I). rMANF+rHSPA5-treated mice also exhibited reduced cleaved caspase 3 foci (as a marker of cardiac injury) following ICI treatment (fig. S11). Hence, our findings suggested that administration of recombinant MANF attenuated myocyte death and immune infiltration in ICI-associated myocarditis, signifying the functional importance of MANF in this disease.

To explore the underlying mechanisms of MANF in attenuating myocarditis, we examined the transcriptional profiles of vehicle or rMANF/rHSPA5-treated hearts based on the ICB treatment (fig. S12A and GSE213468). Compared to the vehicle-treated group, rMANF/rHSPA5-treated hearts increased genes responsible for junction complex organization, Wnt signaling, cell adhesion, and inhibition of epithelial mesenchymal transition (EMT), cellular processes that promote tissue protection against injury (fig. S12, B and C; GSE213468). In addition, enhanced cell adhesion/junction complex organization and reduced EMT are known to improved cell-cell adhesion, inhibiting leukocyte migration (39). Indeed, previous studies indicated that *Manf*-deficiency leads to downregulated genes mostly pertaining to cell adhesion and differentiation (40). Wnt and downstream β-catenin play essential

roles in the proliferation and anti-apoptosis of cardiomyocytes (41). Furthermore, data from other models of myocardial injury suggest that diminished Wnt signaling leads to arrhythmogenic cardiomyopathy (42, 43). We next determined the phosphorylation of LRP6 (Low-density lipoprotein receptor-related protein 6) and β-catenin at S33/S37/T41 upon Wnt3α stimulation in the presence of rMANF or rHSPA5, finding that rMANF, but not rHSPA5 facilitated the Wnt-induced phosphorylation of LRP6 at S1490 and β-catenin at S33/S37/T41 (fig. S12, D to F). The presence of rMANF enhanced the phosphorylation status of these sites (fig. S12, D to F).

ICI effects on sex hormones and transcriptional regulation of MANF and HSPA5

Previous literature has shown a critical role for female hormones, specifically 17 β-estradiol, and male hormones (testosterones) in immune regulation and cardio protection in other settings (44, 45). Since we did not observe any pathology at baseline in our mouse models, we wondered whether ICI treatment might affect the serum concentrations of 17 β-estradiol and testosterone in both male and female animals. Surprisingly, we found that ICI treatment significantly reduced serum 17 β-estradiol concentrations in both males and females 2 weeks after treatment. This effect was observed in both tumor-bearing (female) and non-tumor-bearing (male and female) animals (Fig. 5, A and B). ICI administration showed no effects on the serum concentrations of testosterone progesterone in either male or female animals (Fig. 5, C and D, and fig. S13, A and B). Ovaries and mammary gland tissues of female mice following vehicle or ICI treatment showed no obvious damage (fig. S13C).

In parallel, we established an *in vitro* model using human induced pluripotent stem (iPS) cells-derived cardiomyocytes (iPS-CMs) to further explore the myocyte-specific regulation of MANF/HSPA5 transcription and the potential role of sex hormones in this process. We initially hypothesized that estrogens may suppress MANF/HSPA5, thus predisposing female mice to ICI-myocarditis. Surprisingly, in iPS-CMs, estrogen (E_2) robustly induced mRNA and protein expression of *MANF* and *HSPA5*. Conversely, dihydrotestosterone (DHT) inhibited the expression of *MANF* and *HSPA5* (Fig. 6, A to C). In comparison, treatment of iPS-CMs with pro-inflammatory cytokines, such as IL-6, IFN-γ, or TNF-α, which have been shown to recapitulate inflammatory-mediated cardiac damage, minimally affected *MANF/HSPA5* at the mRNA and protein expression (Fig. 6, A to C). The promoters of *MANF* and *HSPA5* contain consensus sequences for androgen receptor (AR) and estrogen receptor (ER) binding elements (Fig. 6, D and E, and fig. S14, A and B, top panels). Chromatin immunoprecipitation (ChIP) assay indicated the recruitment of AR to the promoters of *MANF* and *HSPA5* in iPS-CMs following DHT treatment (Fig. 6D and fig. S14A). The recruitment of AR to the transcription units following DHT treatment might trigger activation or repression of transcription (46). We confirmed the recruitment of transcription co-repressors NcoR and REST (47) to the promoters of *MANF/HSPA5* upon ligand stimulation (Fig. 6D and fig. S14A). Furthermore, ERβ, but not ERα, was recruited to the promoter regions of *MANF* and *HSPA5* respectively upon E_2 stimulation (Fig. 6E and fig. S14B). The E_2-induced expression of mouse *Manf/Hspa5* occurred in an *Esr2*-dependent manner (Fig. 6, F to H). Similarly, knockout of *Ar* abolished the DHT-triggered repression of *Manf/Hspa5* in neonatal mouse cardiomyocytes (Fig. 6, I to K). Taken together, our findings suggest that ICI treatment results in reduced female hormone concentrations in

blood, serving as a fundamental mechanism underlying the sex disparities of ICI-associated myocarditis. On other hand, estrogens induce *MANF/HSPA5* expression in cardiomyocytes. Therefore, one may hypothesize that hormone-directed therapies following ICI treatment may serve as a therapeutic strategy in attenuating ICI-myocarditis.

We next explored whether hormone-directed therapies may affect the expression of *MANF* and *HSPA5* using our *in vitro* system. We specifically focused on ERβ, since perturbation of ERα may affect anti-tumor effects of cancer therapies, especially since ERα promotes the growth of multiple types of tumors including breast cancer and melanoma (48). On the other hand, it has been suggested that ERβ may act as a tumor suppressor (49). Indeed, LY500307, an ERβ-specific agonist, has been shown to have anti-tumor effects in pre-clinical models of triple negative breast cancer (TNBC) (49). Treatment with LY500307 promoted *MANF* and *HSPA5* expression, which was diminished upon ERβ depletion (Fig. 6, L to N). On the other hand, apalutamide (ARN-509), which associates with AR's ligand binding domain and inhibits AR-dependent transcriptional activity, has recently been approved by the FDA for treating metastatic castration-sensitive prostate cancer (50). ARN-509 antagonizes the DHT-dependent repression of *MANF* and *HSPA5* (Fig. 6, O and P). Hence, the results of our study indicated that the expression of *MANF* and *HSPA5* was activated by E_2 and repressed by DHT, whereby the expression of *MANF* and *HSPA5* were restored upon ERβ agonist or AR deprivation therapy.

Hormone therapies alleviate immunotherapy-associated cardiotoxicity

Our previous experiments showed that transcriptional activity of *MANF* is activated by ERβ and repressed by AR. To test whether hormone therapy can attenuate myocarditis following ICI treatment, tumor-bearing mice were treated with LY500307 or ARN-509 (apalutamide) to stimulate the activation of ERβ signaling or inhibit AR signaling, respectively (Fig. 7A). LY500307 has been suggested to up-regulate the expression of ERβ and diminishes tumor resistance to ICI therapy (51). Female mice harboring EO771 tumors, which represent human triple negative breast cancer, were administered with LY500307 at the time of ICI treatment (Fig. 7A and fig. S15A). LY500307-treated hearts exhibited increased MANF/HSPA5 protein expression, reduced cleaved caspase 3 staining, reduced $CD8^+$ T cell infiltration, and enhanced heart function (Fig. 7, B to F, and fig. S15, B to E). Conversely, RM1 murine prostate cancer-bearing mice were treated with ARN-509 (apalutamide) following ICI treatment. ARN-509 treatment did not affect tumor inhibition by ICI in the RM1-bearing male mice (fig. S15F). ARN-509-treated hearts showed enhanced MANF/HSPA5 expression, decreased cleaved caspase 3 staining intensity, diminished $CD8^+$ T cell infiltration, and improved cardiac contraction (Fig. 7, G to K, and fig. S15, G to J). Taken together, our data suggested that hormone therapy improves the expression of MANF while inhibiting ICI-associated cardiac irAEs.

DISCUSSION

Although immune checkpoint blockade has shown remarkable efficacy in treating multiple cancer types, cardiac irAEs remain a serious concern (52). Alleviating the adverse side effects of ICI treatment without affecting anti-tumor immunity is essential. In this

study, we developed tumor-bearing mouse models of ICI-myocarditis and noted a female predilection to myocarditis, as noted previously in a genetic model of ICI-myocarditis and from preliminary data in the human population. We investigated the underlying cardiac compensatory mechanisms that modulate the cardiac-immune interaction. We identified two factors, MANF and HSPA5, related to unfolded protein response (UPR) which were significantly downregulated in ICI-myocarditis, especially in females. We provided data whereby MANF plays a causal role in modulating myocarditis in these models. We showed that ICI treatment significantly reduced serum concentrations of 17 β-estradiol, especially in female mice, resulting in downregulation of *Manf* and *Hspa5* in the heart. In addition, hormonal therapy using ERβ agonist or androgen deprivation therapy (ADT) attenuated myocarditis via upregulating *Manf* and *Hspa5* expression (fig. S15K). Our findings provide clinical considerations that may broaden the utility and viability of ICI therapies, which could allow this treatment strategy to benefit a wider range of cancer patients.

The mechanism of ICI-associated myocarditis remains elusive. Multiple possible immune-mediated mechanisms have been proposed including shared antigens between the tumor and cardiomyocytes (53). In addition, immune checkpoints including PD-1/PD-L1 (and possibly CTLA-4) pathways regulate T cell interactions with the heart under physiological conditions. However, the mechanisms underlying the gender disparities of myocarditis are currently unclear. Here we identify MANF and HSPA5 are critical in attenuating myocardial inflammation in ICI-myocarditis. We show that *MANF* and *HSPA5* were transcriptionally enhanced by female hormones. Conversely, male hormones inhibited the expression of these genes. Administration of recombinant MANF restored the heart function of ICI-treated mice. Though HSPA5 expression was also decreased, our findings suggested that HSPA5 were downregulated similarly in both male and female ICI-treated hearts. Hence, our findings suggested that MANF might play a critical role in the gender disparities of ICI-associated myocarditis in our mouse model. The presence of rMANF and rHSPA5 exhibited minimal effects on tumor infiltrating $CD8^+$ T cells and macrophages, leading to unaffected anti-tumor immunity. However, a role for HSPA5 in ICI-associated cardiotoxicity cannot be ruled out.

Our findings support that hormone therapies, including ERβ agonists or androgen depletion, effectively restored the cardiac expression of MANF/HSPA5, reduced the infiltration of $CD8^+$ T cells and macrophages in the heart, and prevented the apoptosis of the myocardium. Genetic evidence indicated that mice with *ERβ* knockout, but not *ERα* knockout, are susceptible to ischemia/reperfusion injury (54). Erβ-specific agonists have been shown to be cardioprotective against ischemia-reperfusion injury (55). Hence, combining an ERβ-specific agonist, or androgen deprivation therapies with immunotherapy might improve anti-tumor effects of ICIs and reduce the incidence of ICI-associated cardiotoxicity (56, 57).

The irAEs of immunotherapy involve endocrinopathies, which include primary adrenal insufficiency, hypophysitis, thyroid dysfunction, diabetes, and others (58). Chemotherapies also reduce 17 β-estradiol concentration (59). Although testosterone and E_2 concentrations in cancer patients' serum are not typically evaluated in clinical settings, we demonstrated the tumor burden-independent downregulation of mouse serum E_2 concentration in female mice following ICI treatment. The potential mechanisms of ICI-induced reduction of estradiol are

unknown. One possibility is that ICI could result in hormone suppression via the ovaries or pituitaries, but this would mean a more general change in hormone concentration and clearly requires further investigation. Monitoring the hormone concentration of cancer patients undergoing ICI treatments could therefore be a crucial clinical consideration. The potential difference of rodent and human sex hormone metabolism (60) shall be considered.

Several lines of evidence suggest that MANF has tissue-protective properties. MANF has been shown to negatively correlate with atrial apoptosis in atrial fibrillation (61). The expression of MANF is induced by ischemic conditions and protects against ischemic damage (35, 62). Expression of exogenous MANF via an AAV-mediated method has been suggested to improve neuronal functional recovery post-stroke (63). Recombinant MANF alleviates simulated ischemia reperfusion-associated injury (62) and promotes neuronal differentiation post-stroke (64). Cardiokine therapies could serve as potential strategies for treating cardiac irAE. Three strategies could be considered for restoring the expression of *Manf/Hspa5* in the heart: AAV-mediated gene therapy, administration of recombinant protein, and transcriptional upregulation of these genes with hormone therapies. Given potential concerns about unspecific incorporation of therapeutic genes into the genome (65) and the successful application of recombinant MANF against neurodegenerative disease (64), we considered that *in vivo* delivery of recombinant MANF might be suitable for cancer patients who have a high risk of heart failure and are undergoing ICI treatment. Preclinical PK and toxicology studies suggested that injection of MANF protein results in robust infusion *in vivo* (64). The tissue half-life of MANF could be 5.5h in rats (66). Repeated infusion of MANF showed well-tolerated clinical signs, undetectable pathology parameters, and normal neurological evaluations with minimal carcinogenicity in male and female rhesus macaques (66). Hence, the administration of recombinant MANF might provide a convenient, safe, and effective strategy for combatting ICI-induced heart defects. Building upon this, future work will explore the mechanisms by which not only ICI treatment decreases estrogen signaling / 17β-estradiol but also MANF/HSPA5 decreases apoptosis and lymphocyte infiltration in hear tissue.

MATERIALS AND METHODS

Study design

The objective of this study was to develop a preclinical strategy to overcome female susceptibility to ICI-associated myocarditis using both pharmacological and genetic mouse models that recapitulated this complication. We defined the molecular mechanism by which ICI induces the heart-specific downregulation of MANF and HSPA5. Preclinical studies were further performed to evaluate the therapeutic effects of hormonal therapies, which restore the MANF and HSPA5 levels upon alleviation of ICI-associated myocarditis. A comprehensive approach that included RNA-seq, genetic knockout mouse model, iPSC-differentiated cardiomyocytes, mouse ECG assays, and so forth was applied to increase the rigor of this study. We obtained primary human ICI-Myocarditis heart tissues, approved by the Institutional Review Board of Vanderbilt University and UCSF. All *in vivo* experiments were performed following the guidance of the Institutional Animal Care and Use Committee. Mice were randomized before each experiment, but investigators were not

blinded to group allocation. For other assays, at least two independent experiments were performed with biological replicates or triplicates. Sample size in experiments was specified in each figure legend. We did not exclude samples or animals. For every figure, statistical tests are justified as appropriate.

In vivo xenograft murine models and treatment

All animal-based research was performed in accordance with the guidelines and requirements set forth by the Public Health Service (PHS) Policy on Humane Care and Use of Laboratory Animals, the U.S. Department of Health and Human Services Guide for the Care and Use of Laboratory Animals, and the Animal Welfare Act of 1966 as amended by the Institutional Animal Care and Use Committee (IACUC) of the University of Texas M.D. Anderson Cancer Center (MDACC). Male and female 6–8 weeks old wild type C57/BL6J mice, *Esr2* knockout mice (B6.129P2-Esr2tm1Unc/J) and conditional *Ar* knockout mice (B6.129S1-Artm2.1Reb/J) were obtained from the Jackson Laboratory. The animals were grouped randomly, and 3–5 mice were put into each cage. The animals were implanted with respective tumor cells in the unit of cages, which were randomly selected. Tumor size was measured every 3 days using a caliper, and tumor volume was calculated using the standard formula: $0.54\times L\times W^2$, where L is the longest diameter and W is the shortest diameter. Immune checkpoint blockade treatment was started when tumor volume reached 200–250 mm^3 using anti-mouse PD-1 [25 mg/kg, intraperitoneal (i.p.), every 3 days (q3)] combined with anti-mouse CTLA-4 antibody (25 mg/kg, i.p., q3). The control group was injected with an equal dosage of rat IgG2a isotype (50 mg/kg, i.p., q3).

HEK293T cells-purified recombinant c-Myc-tagged mouse HSPA5 (aa. 1–655) was obtained from Origene Technologies inc (Cat#: TP509794) and was purified with immobilized metal affinity chromatography (IMAC), with over 90% purity. HEK293-purified recombinant His-tagged mouse MANF (aa. 1–179) was obtained from Sino Biological (Cat#: 50954-M08H), with over 90% purity. C-Myc-tagged HSPA5 [7.8 μg/kg, i.p., everyday (qd)] and His-tagged MANF protein (2 μg/kg, i.p., qd) were resuspended in PBS pH 7.4 and were used to treat the mice from 7 days before tumor cell inoculation till the end of the experiment.

The female mice were treated with PBS or LY500307 (ip injection, 5 mg/kg) from the same day of tumor inoculation until the end of the experiment. The male mice were treated with the vehicle or ARN-509 (10 mg/kg, oral gavage, daily) from the same day of tumor cell inoculation until the end of the experiment. All animals were housed with a 12 h light/ 12 h dark cycle in the animal facility with free access to water and food. To obtain unbiased and reliable results, at least five mice were used in each group. Sample size was indicated in corresponding figure legend.

The genetic *Ctla4* haploinsufficiency in the absence of *Pdcd1* mouse model

Mice derived from a $Ctla4^{+/-}$ $Pdcd1^{-/-}$ by $Ctla4^{+/+}$ $Pdcd1^{-/-}$ breeding performed at the Vanderbilt University Medical Center (VUMC) vivarium to generate progeny animals. All mice were genotyped at 3 weeks old, and their date of death were recorded as previously exhaustively described (18). For the generation of survival curve, events were defined as either death (i.e., mice found dead) or identification of mice by veterinary staff as requiring

euthanasia (e.g., due to lethargy, moribund, dyspnea). All experiments were performed in accordance with the Vanderbilt University Medical Center IACUC guidelines.

Statistical analysis

The experiment was set up to use 3–12 samples/repeats per experiment/group/condition. Each of these experiments was independently repeated 3–8 times. Results are reported as mean ± standard error of the mean (S.E.M.) or standard deviation (SD). Each exact n value is indicated in the corresponding figure legend. Pearson's correlation analysis was implemented for statistical analysis of the correlation between the intensity of cells marker and individual protein concentration. Kaplan-Meier survival curves were compared using the log-rank test. Statistical analysis was performed using GraphPad Prism version 9.0 (GraphPad software). The difference in multiple groups was estimated by one-way or two-way ANOVA analysis, and Student's t-test was used to estimate of the difference in only two groups. (*) $P < 0.05$, (**) $P < 0.01$, (***) $P < 0.001$, (****) $P < 0.0001$; ns is not significant, as indicated in individual figures. Individual data value is reported in data file S1.

Murine model of acute ischemic cardiac injury

Myocardial infarction was performed by ligating the left anterior descending (LAD) coronary artery following open thoracotomy as described (67).

Samples of human ICI-myocarditis

Our group has established an international registry of patients with ICI-associated myocarditis using a Research Electronic Data Capture web-based platform with Institutional Review Board approval (Institutional Review Board No. 181337; URL: http://www.clinicaltrials.gov; Unique identifier: NCT04294771) (15, 68). At Vanderbilt University Medical Center and at University of California, San Francisco (UCSF), we have obtained formalin-fixed paraffin embedded tissue from patients with various forms of myocarditis including ICI-associated myocarditis as well as unused healthy donor heart samples (Institutional Review Board no. 201926), as previous described (69). The clinical information of human tissue samples was included in the table S2. Antibodies are listed in table S3.

Tissue collection and immunohistochemistry (IHC) staining

Unless otherwise indicated, the mice were fasted for 4–6 h, anesthetized with isoflurane, blood was collected by heart puncture, and then mice were euthanized. H&E staining was performed to characterize cardiac muscle pathology. Fluorescent multiplex immunohistochemistry (mIHC) and regular immunohistochemistry (IHC) staining were performed by using antibodies as indicated in table S3. All immune-stained slides were scanned with the Vectra Polaris Quantitative Pathology Imaging System (PerkinElmer) for quantification by a digital image analysis. The quantification of IHC staining density was performed by Image-pro plus 6.0 software (Media Cybernetics) and calculated based on the average staining intensity.

AAV-meditated *Manf* KO

To evaluate the cardiac protective function of MANF, we knocked out *Manf* in adult C57BL/6J mice using AAV as previously described with minor modification (70). saCas9 under the control of the cardiac muscle troponin T promoter (cTnT) (AAV-cTnT-saCas9), and the sagRNA with scramble sequence, or targeting *Manf* exon 2, under the control of U6 promoter (AAV-Scr-sagRNA, AAV-*Manf*-sagRNA) were generated (AAV vector construction services provided by VectorBuilder). Scramble and *Manf* sagRNA sequence were included in the table S4 These viral vectors were sent to the Institutional Vector Core at the MD Anderson Cancer Center for packaging (AAV9 serotype, 1.5×10^{13} vg ml^{-1}). For AAV intra-cardiac injection, 2×10^{11} viral genomes of each AAV (AAV9 serotype, 1.5×10^{13} vg ml^{-1}) were diluted in 50 μl saline, and were injected directly into the left ventricle of each mice at age of 5-week-old. 3 weeks post the AAV administration, the animals were subcutaneously inoculated with B16F10 cells. ICI and the IgG isotope treatment was conducted when the tumor volume reach to 200–250 mm^3.

Tumor cell line culture

The mouse breast adenocarcinoma cell line EO771, mouse colon adenocarcinoma cell line MC38, mouse melanoma cell line B16F10, and mouse prostate cancer RM1 cells were purchased from the American Type Culture Collection (ATCC), and the tumor cells were maintained in the respective optimal complete growth medium according to the instruction of ATCC. 1×10^5 EO771 were injected into the mammary fat pad. 1×10^5 MC38, 0.5×10^5 B16F10 or 1×10^5 RM1 cells were inoculated subcutaneously into the right flank of the mice.

Induced pluripotent stem cells (iPSCs) maintenance and differentiation

The human iPSC studies were approved by the HEIP Stem Cell committee of the University of Texas, MD Anderson Cancer Center. The HSCC-022iPS cell line from an 11-year-old healthy female donor was obtained from the Human Stem Cell Core (HSCC) (Baylor College of Medicine). It was cultured in hESC-Qualified Matrigel (Corning)-coated plates and maintained in mTeSR plus medium (Stemcell Technologies). The iPS cells were then differentiated to cardiomyocytes by using the STEMdiff Cardiomyocyte Differentiation Kit (Stemcell Technologies) according to manufacture instruction. HiPS-CMs were treated with β-Estradiol (10 nM, Sigma-Aldrich), 5α-Dihydrotestosterone (10 nM, Sigma-Aldrich), IL-6 (10 ng/ml PeproTech), TNF-α (10 ng/ml PeproTech), IFN-γ (10 ng/ml PeproTech), LY500307 (10 nM, APExBIO), or ARN-509 (10 nM, Cayman Chemical) for 1 hr or as indicated in the figure legends.

Bulk RNA-seq, data analysis and QPCR

RNA-seq was performed by Illumina HiSeq 2000 with a 150bp paired-end read. Reads were aligned to the mouse genome (Ensembl mm10 mouse genome) using HISAT2 (V 2.1.0) (71) with default parameters, and reads were assigned to genes using feature Counts (V 1.6.5) (71). Differential expression analysis and FPKM (fragments per kilo-base of exon per million fragments) calculation of genes in each sample were performed by edgeR (72). Genes with an FDR (false discovery rate) adjusted by the method of Benjamini and Hochberg < 0.1 and a fold change > 1.5 were assigned as significantly differentially

expressed genes (DEGs) between the ICI and IgG samples. Significantly DEGs were subjected to pathway enrichment by R package “clusterProfiler” (73). Venn diagrams shown the overlap of significantly DEGs were completed by R package “venn”. Heatmaps of significantly DEGs were plotted by R package “heatmap”. The raw RNA-seq data for this manuscript is available at GEO under the accession number GSE145573 and GSE213468. For bulk RNA-seq of mice following myocardial infarct, the data GSE151834 in NCBI GEO dataset (74) were analyzed. Reads were aligned to the mouse reference genome (mm10) using STAR aligner and used to quantify normalized expression values (RPKM) for annotated genes (Ensembl v.86). Normalized expression levels (RPKM) were used for gene expression visualizations.

RNA isolation, qRT-PCR, cell lysis, ChIP and immunoblotting

Total RNA was isolated from cells using RNeasy Mini Kit (QIAGEN) following the manufacturer’s protocol. First-strand cDNA synthesis from total RNA was carried out using iScript Reverse Transcription Supermix for RT-qPCR (Bio-Rad). Alternatively, cDNAs were generated using iScript cDNA Synthesis Kit (BioRad) and qPCR was performed. Primer sequences are described in table S4. ChIP assays were performed as previously described (75). Primers using for ChIP assays were included in table S4. Cells were homogenized in 1×RIPA buffer (EMD Millipore) supplemented with Protease/ Phosphatase Inhibitor Cocktail (Pierce, Thermo Scientific), Panobinostat (Selleck chemicals) and Methylstat (Sigma-Aldrich). Lysates were cleared by centrifugation at 13,000 rpm for 15 minutes at 4 °C. Supernatants were analyzed for immunoprecipitation with the indicated antibodies as listed in table S3 and the immunoprecipitated proteins were further subjected to immunoblotting detection.

Supplementary Material

Refer to Web version on PubMed Central for supplementary material.

Acknowledgments

We would like to thank the Human Stem Cell Core of Baylor College of Medicine for technical assistance with stem cell reprogramming, maintenance, and differentiation.

Funding:

This work was supported by MDACC Internal Research Grant, MDACC Bridge fund, MDACC Faculty Scholar Award, CPRIT (RP200423) and AACR-The Mark Foundation SOP Grants (20-60-51 Yang) (to L.Q.Y.); NIH (R01CA218025, R01CA231011), CPRIT (RP180259), Department of Defense (DoD) (BC180196) grants (to C.R.L.) and NIH (R01HL141466, R01HL155990, R01HL156021) grants (to J.J.M.).

Data and material availability:

All data associated with this study are in the paper or supplementary materials. The raw RNA-seq data for this manuscript is available at GEO under the accession number GSE145573 and GSE213468. The hiPSs were obtained from the Coriell Institute for Medical Research and are subject to restrictions on redistribution and sharing. *Ctla4*- and *Pdcd1*-knockout transgenic mice are available from J.J.M. under a material transfer agreement with the University of Texas MD Anderson Cancer Center.

REFERENCES AND NOTES

1. Pardoll DM, The blockade of immune checkpoints in cancer immunotherapy. Nat Rev Cancer 12, 252–264 (2012). [PubMed: 22437870]
2. Sharpe AH, Pauken KE, The diverse functions of the PD1 inhibitory pathway. Nat Rev Immunol 18, 153–167 (2018). [PubMed: 28990585]
3. Ribas A, Tumor immunotherapy directed at PD-1. N Engl J Med 366, 2517–2519 (2012). [PubMed: 22658126]
4. Chen L, Han X, Anti-PD-1/PD-L1 therapy of human cancer: past, present, and future. J Clin Invest 125, 3384–3391 (2015). [PubMed: 26325035]
5. Cristescu R, Mogg R, Ayers M, Albright A, Murphy E, Yearley J, Sher X, Liu XQ, Lu H, Nebozhyn M, Zhang C, Lunceford JK, Joe A, Cheng J, Webber AL, Ibrahim N, Plimack ER, Ott PA, Seiwert TY, Ribas A, McClanahan TK, Tomassini JE, Loboda A, Kaufman D, Pan-tumor genomic biomarkers for PD-1 checkpoint blockade-based immunotherapy. Science 362, (2018).
6. Herbst RS, Soria JC, Kowanetz M, Fine GD, Hamid O, Gordon MS, Sosman JA, McDermott DF, Powderly JD, Gettinger SN, Kohrt HE, Horn L, Lawrence DP, Rost S, Leabman M, Xiao Y, Mokatrin A, Koeppen H, Hegde PS, Mellman I, Chen DS, Hodi FS, Predictive correlates of response to the anti-PD-L1 antibody MPDL3280A in cancer patients. Nature 515, 563–567 (2014). [PubMed: 25428504]
7. Iwai Y, Ishida M, Tanaka Y, Okazaki T, Honjo T, Minato N, Involvement of PD-L1 on tumor cells in the escape from host immune system and tumor immunotherapy by PD-L1 blockade. Proc Natl Acad Sci U S A 99, 12293–12297 (2002). [PubMed: 12218188]
8. Larkin J, Chiarion-Sileni V, Gonzalez R, Grob JJ, Cowey CL, Lao CD, Schadendorf D, Dummer R, Smylie M, Rutkowski P, Ferrucci PF, Hill A, Wagstaff J, Carlino MS, Haanen JB, Maio M, Marquez-Rodas I, McArthur GA, Ascierto PA, Long GV, Callahan MK, Postow MA, Grossmann K, Sznol M, Dreno B, Bastholt L, Yang A, Rollin LM, Horak C, Hodi FS, Wolchok JD, Combined Nivolumab and Ipilimumab or Monotherapy in Untreated Melanoma. N Engl J Med 373, 23–34 (2015). [PubMed: 26027431]
9. Johnson DB, Reynolds KL, Sullivan RJ, Balko JM, Patrinely JR, Cappelli LC, Naidoo J, Moslehi JJ, Immune checkpoint inhibitor toxicities: systems-based approaches to improve patient care and research. Lancet Oncol 21, e398–e404 (2020). [PubMed: 32758477]
10. Martins F, Sofiya L, Sykiotis GP, Lamine F, Maillard M, Fraga M, Shabafrouz K, Ribi C, Cairoli A, Guex-Crosier Y, Kuntzer T, Michielin O, Peters S, Coukos G, Spertini F, Thompson JA, Obeid M, Adverse effects of immune-checkpoint inhibitors: epidemiology, management and surveillance. Nat Rev Clin Oncol 16, 563–580 (2019). [PubMed: 31092901]
11. Moslehi JJ, Salem JE, Sosman JA, Lebrun-Vignes B, Johnson DB, Increased reporting of fatal immune checkpoint inhibitor-associated myocarditis. Lancet 391, 933 (2018).
12. Salem A, Asselin MC, Reymen B, Jackson A, Lambin P, West CML, O'Connor JPB, Faivre-Finn C, Targeting Hypoxia to Improve Non-Small Cell Lung Cancer Outcome. J Natl Cancer Inst 110, (2018).
13. Moslehi J, Lichtman AH, Sharpe AH, Galluzzi L, Kitsis RN, Immune checkpoint inhibitor-associated myocarditis: manifestations and mechanisms. J Clin Invest 131, (2021).
14. Mahmood SS, Fradley MG, Cohen JV, Nohria A, Reynolds KL, Heinzerling LM, Sullivan RJ, Damrongwatanasuk R, Chen CL, Gupta D, Kirchberger MC, Awadalla M, Hassan MZO, Moslehi JJ, Shah SP, Ganatra S, Thavendiranathan P, Lawrence DP, Groarke JD, Neilan TG, Myocarditis in Patients Treated With Immune Checkpoint Inhibitors. J Am Coll Cardiol 71, 1755–1764 (2018). [PubMed: 29567210]
15. Power JR, Alexandre J, Choudhary A, Ozbay B, Hayek S, Asnani A, Tamura Y, Aras M, Cautela J, Thuny F, Gilstrap L, Arangalage D, Ewer S, Huang S, Deswal A, Palaskas NL, Finke D, Lehman L, Ederhy S, Moslehi J, Salem JE, International ICIMR, Electrocardiographic Manifestations of Immune Checkpoint Inhibitor Myocarditis. Circulation 144, 1521–1523 (2021). [PubMed: 34723640]
16. Bonaca MP, Olenchock BA, Salem JE, Wiviott SD, Ederhy S, Cohen A, Stewart GC, Choueiri TK, Di Carli M, Allenbach Y, Kumbhani DJ, Heinzerling L, Amiri-Kordestani L, Lyon AR,

Thavendiranathan P, Padera R, Lichtman A, Liu PP, Johnson DB, Moslehi J, Myocarditis in the Setting of Cancer Therapeutics: Proposed Case Definitions for Emerging Clinical Syndromes in Cardio-Oncology. Circulation 140, 80–91 (2019). [PubMed: 31390169]

17. Michel L, Helfrich I, Hendgen-Cotta UB, Mincu RI, Korste S, Mrotzek SM, Spomer A, Odersky A, Rischpler C, Herrmann K, Umutlu L, Coman C, Ahrends R, Sickmann A, Loffek S, Livingstone E, Ugurel S, Zimmer L, Gunzer M, Schadendorf D, Totzeck M, Rassaf T, Targeting early stages of cardiotoxicity from anti-PD1 immune checkpoint inhibitor therapy. Eur Heart J 43, 316–329 (2022). [PubMed: 34389849]
18. Wei SC, Meijers WC, Axelrod ML, Anang NAS, Screever EM, Wescott EC, Johnson DB, Whitley E, Lehmann L, Courand PY, Mancuso JJ, Himmel LE, Lebrun-Vignes B, Wleklinski MJ, Knollmann BC, Srinivasan J, Li Y, Atolagbe OT, Rao X, Zhao Y, Wang J, Ehrlich LIR, Sharma P, Salem JE, Balko JM, Moslehi JJ, Allison JP, A Genetic Mouse Model Recapitulates Immune Checkpoint Inhibitor-Associated Myocarditis and Supports a Mechanism-Based Therapeutic Intervention. Cancer Discov 11, 614–625 (2021). [PubMed: 33257470]
19. Xia W, Chen H, Chen D, Ye Y, Xie C, Hou M, PD-1 inhibitor inducing exosomal miR-34a-5p expression mediates the cross talk between cardiomyocyte and macrophage in immune checkpoint inhibitor-related cardiac dysfunction. J Immunother Cancer 8, (2020).
20. Bockstahler M, Fischer A, Goetzke CC, Neumaier HL, Sauter M, Kespohl M, Muller AM, Meckes C, Salbach C, Schenk M, Heuser A, Landmesser U, Weiner J, Meder B, Lehmann L, Kratzer A, Klingel K, Katus HA, Kaya Z, Beling A, Heart-Specific Immune Responses in an Animal Model of Autoimmune-Related Myocarditis Mitigated by an Immunoproteasome Inhibitor and Genetic Ablation. Circulation 141, 1885–1902 (2020). [PubMed: 32160764]
21. Du S, Zhou L, Alexander GS, Park K, Yang L, Wang N, Zaorsky NG, Ma X, Wang Y, Dicker AP, Lu B, PD-1 Modulates Radiation-Induced Cardiac Toxicity through Cytotoxic T Lymphocytes. J Thorac Oncol 13, 510–520 (2018). [PubMed: 29247829]
22. Hu JR, Florido R, Lipson EJ, Naidoo J, Ardehali R, Tocchetti CG, Lyon AR, Padera RF, Johnson DB, Moslehi J, Cardiovascular toxicities associated with immune checkpoint inhibitors. Cardiovasc Res 115, 854–868 (2019). [PubMed: 30715219]
23. Zamami Y, Niimura T, Okada N, Koyama T, Fukushima K, Izawa-Ishizawa Y, Ishizawa K, Factors Associated With Immune Checkpoint Inhibitor-Related Myocarditis. JAMA Oncol 5, 1635–1637 (2019). [PubMed: 31436802]
24. Valpione S, Pasquali S, Campana LG, Piccin L, Mocellin S, Pigozzo J, Chiarion-Sileni V, Sex and interleukin-6 are prognostic factors for autoimmune toxicity following treatment with anti-CTLA4 blockade. J Transl Med 16, 94 (2018). [PubMed: 29642948]
25. Fairweather D, Cooper LT Jr., Blauwet LA, Sex and gender differences in myocarditis and dilated cardiomyopathy. Curr Probl Cardiol 38, 7–46 (2013). [PubMed: 23158412]
26. Shimano M, Ouchi N, Walsh K, Cardiokines: recent progress in elucidating the cardiac secretome. Circulation 126, e327–332 (2012). [PubMed: 23169257]
27. Kempf T, Eden M, Strelau J, Naguib M, Willenbockel C, Tongers J, Heineke J, Kotlarz D, Xu J, Molkentin JD, Niessen HW, Drexler H, Wollert KC, The transforming growth factor-beta superfamily member growth-differentiation factor-15 protects the heart from ischemia/reperfusion injury. Circ Res 98, 351–360 (2006). [PubMed: 16397141]
28. Dschietzig TB, Myostatin - From the Mighty Mouse to cardiovascular disease and cachexia. Clin Chim Acta 433, 216–224 (2014). [PubMed: 24680839]
29. Zhang J, Zhang X, Cui Y, Cui L, Zhao P, Macrophage migration inhibitory factor knockout attenuates endotoxin-induced cardiac dysfunction in mice. Kardiol Pol 76, 871–880 (2018). [PubMed: 29350381]
30. Grabie N, Lichtman AH, Padera R, T cell checkpoint regulators in the heart. Cardiovasc Res 115, 869–877 (2019). [PubMed: 30721928]
31. McIntyre RE, Buczacki SJ, Arends MJ, Adams DJ, Mouse models of colorectal cancer as preclinical models. Bioessays 37, 909–920 (2015). [PubMed: 26115037]
32. Fidler IJ, From here to there; a life based on migration. An interview with Isaiah J. Fidler. Int J Dev Biol 48, 457–462 (2004). [PubMed: 15349820]

33. Johnstone CN, Smith YE, Cao Y, Burrows AD, Cross RS, Ling X, Redvers RP, Doherty JP, Eckhardt BL, Natoli AL, Restall CM, Lucas E, Pearson HB, Deb S, Britt KL, Rizzitelli A, Li J, Harmey JH, Pouliot N, Anderson RL, Functional and molecular characterisation of EO771.LMB tumours, a new C57BL/6-mouse-derived model of spontaneously metastatic mammary cancer. Dis Model Mech 8, 237–251 (2015). [PubMed: 25633981]
34. Blanco-Dominguez R, Sanchez-Diaz R, de la Fuente H, Jimenez-Borreguero LJ, Matesanz-Marin A, Relano M, Jimenez-Alejandre R, Linillos-Pradillo B, Tsilingiri K, Martin-Mariscal ML, Alonso-Herranz L, Moreno G, Martin-Asenjo R, Garcia-Guimaraes MM, Bruno KA, Dauden E, Gonzalez-Alvaro I, Villar-Guimerans LM, Martinez-Leon A, Salvador-Garicano AM, Michelhaugh SA, Ibrahim NE, Januzzi JL, Kottwitz J, Iliceto S, Plebani M, Basso C, Baritussio A, Seguso M, Marcolongo R, Ricote M, Fairweather D, Bueno H, Fernandez-Friera L, Alfonso F, Caforio ALP, Pascual-Figal DA, Heidecker B, Luscher TF, Das S, Fuster V, Ibanez B, Sanchez-Madrid F, Martin P, A Novel Circulating MicroRNA for the Detection of Acute Myocarditis. N Engl J Med 384, 2014–2027 (2021). [PubMed: 34042389]
35. Glembotski CC, Functions for the cardiomyokine, MANF, in cardioprotection, hypertrophy and heart failure. J Mol Cell Cardiol 51, 512–517 (2011). [PubMed: 20970425]
36. Zhang PL, Lun M, Teng J, Huang J, Blasick TM, Yin L, Herrera GA, Cheung JY, Preinduced molecular chaperones in the endoplasmic reticulum protect cardiomyocytes from lethal injury. Ann Clin Lab Sci 34, 449–457 (2004). [PubMed: 15648788]
37. Glembotski CC, Thuerauf DJ, Huang C, Vekich JA, Gottlieb RA, Doroudgar S, Mesencephalic astrocyte-derived neurotrophic factor protects the heart from ischemic damage and is selectively secreted upon sarco/endoplasmic reticulum calcium depletion. J Biol Chem 287, 25893–25904 (2012). [PubMed: 22637475]
38. Chadwick AC, Musunuru K, Genome Editing for the Study of Cardiovascular Diseases. Curr Cardiol Rep 19, 22 (2017). [PubMed: 28220462]
39. Muller WA, Getting leukocytes to the site of inflammation. Vet Pathol 50, 7–22 (2013). [PubMed: 23345459]
40. Bell PA, Dennis EP, Hartley CL, Jackson RM, Porter A, Boot-Handford RP, Pirog KA, Briggs MD, Mesencephalic astrocyte-derived neurotropic factor is an important factor in chondrocyte ER homeostasis. Cell Stress Chaperones 24, 159–173 (2019). [PubMed: 30543055]
41. Guo X, Gu X, Hareshwaree S, Rong X, Li L, Chu M, Induced pluripotent stem cell-conditional medium inhibits H9C2 cardiomyocytes apoptosis via autophagy flux and Wnt/beta-catenin pathway. J Cell Mol Med 23, 4358–4374 (2019). [PubMed: 30957422]
42. Lorenzon A, Calore M, Poloni G, De Windt LJ, Braghetta P, Rampazzo A, Wnt/beta-catenin pathway in arrhythmogenic cardiomyopathy. Oncotarget 8, 60640–60655 (2017). [PubMed: 28948000]
43. Gillers BS, Chiplunkar A, Aly H, Valenta T, Basler K, Christoffels VM, Efimov IR, Boukens BJ, Rentschler S, Canonical wnt signaling regulates atrioventricular junction programming and electrophysiological properties. Circ Res 116, 398–406 (2015). [PubMed: 25599332]
44. Klein SL, Flanagan KL, Sex differences in immune responses. Nat Rev Immunol 16, 626–638 (2016). [PubMed: 27546235]
45. Takahashi T, Iwasaki A, Sex differences in immune responses. Science 371, 347–348 (2021). [PubMed: 33479140]
46. Heemers HV, Tindall DJ, Androgen receptor (AR) coregulators: a diversity of functions converging on and regulating the AR transcriptional complex. Endocr Rev 28, 778–808 (2007). [PubMed: 17940184]
47. Perissi V, Jepsen K, Glass CK, Rosenfeld MG, Deconstructing repression: evolving models of co-repressor action. Nat Rev Genet 11, 109–123 (2010). [PubMed: 20084085]
48. Caiazza F, Ryan EJ, Doherty G, Winter DC, Sheahan K, Estrogen receptors and their implications in colorectal carcinogenesis. Front Oncol 5, 19 (2015). [PubMed: 25699240]
49. Austin D, Hamilton N, Elshimali Y, Pietras R, Wu Y, Vadgama J, Estrogen receptor-beta is a potential target for triple negative breast cancer treatment. Oncotarget 9, 33912–33930 (2018). [PubMed: 30338035]

50. Clegg NJ, Wongvipat J, Joseph JD, Tran C, Ouk S, Dilhas A, Chen Y, Grillot K, Bischoff ED, Cai L, Aparicio A, Dorow S, Arora V, Shao G, Qian J, Zhao H, Yang G, Cao C, Sensintaffar J, Wasielewska T, Herbert MR, Bonnefous C, Darimont B, Scher HI, Smith-Jones P, Klang M, Smith ND, De Stanchina E, Wu N, Ouerfelli O, Rix PJ, Heyman RA, Jung ME, Sawyers CL, Hager JH, ARN-509: a novel antiandrogen for prostate cancer treatment. Cancer Res 72, 1494–1503 (2012). [PubMed: 22266222]
51. Huang S, Zhou N, Zhao L, Gimple RC, Ahn YH, Zhang P, Wang W, Shao B, Yang J, Zhang Q, Zhao S, Jiang X, Chen Z, Zeng Y, Hu H, Gustafsson JA, Zhou S, Pharmacological Activation of Estrogen Receptor Beta Overcomes Tumor Resistance to Immune Checkpoint Blockade Therapy. iScience 23, 101458 (2020). [PubMed: 32861994]
52. Gaynor N, Crown J, Collins DM, Immune checkpoint inhibitors: Key trials and an emerging role in breast cancer. Semin Cancer Biol 79, 44–57 (2022). [PubMed: 32623044]
53. Johnson DB, Balko JM, Compton ML, Chalkias S, Gorham J, Xu Y, Hicks M, Puzanov I, Alexander MR, Bloomer TL, Becker JR, Slosky DA, Phillips EJ, Pilkinton MA, Craig-Owens L, Kola N, Plautz G, Reshef DS, Deutsch JS, Deering RP, Olenchock BA, Lichtman AH, Roden DM, Seidman CE, Koralnik IJ, Seidman JG, Hoffman RD, Taube JM, Diaz LA Jr., Anders RA, Sosman JA, Moslehi JJ, Fulminant Myocarditis with Combination Immune Checkpoint Blockade. N Engl J Med 375, 1749–1755 (2016). [PubMed: 27806233]
54. Gabel SA, Walker VR, London RE, Steenbergen C, Korach KS, Murphy E, Estrogen receptor beta mediates gender differences in ischemia/reperfusion injury. J Mol Cell Cardiol 38, 289–297 (2005). [PubMed: 15698835]
55. Nikolic I, Liu D, Bell JA, Collins J, Steenbergen C, Murphy E, Treatment with an estrogen receptor-beta-selective agonist is cardioprotective. J Mol Cell Cardiol 42, 769–780 (2007). [PubMed: 17362982]
56. Guan X, Polesso F, Wang C, Sehrawat A, Hawkins RM, Murray SE, Thomas GV, Caruso B, Thompson RF, Wood MA, Hipfinger C, Hammond SA, Graff JN, Xia Z, Moran AE, Androgen receptor activity in T cells limits checkpoint blockade efficacy. Nature 606, 791–796 (2022). [PubMed: 35322234]
57. Jiang G, Shi L, Zheng X, Zhang X, Wu K, Liu B, Yan P, Liang X, Yu T, Wang Y, Cai X, Androgen receptor affects the response to immune checkpoint therapy by suppressing PD-L1 in hepatocellular carcinoma. Aging (Albany NY) 12, 11466–11484 (2020). [PubMed: 32579541]
58. Chang LS, Barroso-Sousa R, Tolaney SM, Hodi FS, Kaiser UB, Min L, Endocrine Toxicity of Cancer Immunotherapy Targeting Immune Checkpoints. Endocr Rev 40, 17–65 (2019). [PubMed: 30184160]
59. Yu B, Douglas N, Ferin MJ, Nakhuda GS, Crew K, Lobo RA, Hershman DL, Changes in markers of ovarian reserve and endocrine function in young women with breast cancer undergoing adjuvant chemotherapy. Cancer 116, 2099–2105 (2010). [PubMed: 20187091]
60. Nilsson ME, Vandenput L, Tivesten A, Norlen AK, Lagerquist MK, Windahl SH, Borjesson AE, Farman HH, Poutanen M, Benrick A, Maliqueo M, Stener-Victorin E, Ryberg H, Ohlsson C, Measurement of a Comprehensive Sex Steroid Profile in Rodent Serum by High-Sensitive Gas Chromatography-Tandem Mass Spectrometry. Endocrinology 156, 2492–2502 (2015). [PubMed: 25856427]
61. Wang C, Yu S, Bao Q, Qiang W, Wu C, Zhang C, Jiang Y, Cai Y, Huang D, Chen Y, Hou C, Wang D, Circulating Mesencephalic Astrocyte-Derived Neurotrophic Factor Negatively Correlates With Atrial Apoptosis in Human Chronic Atrial Fibrillation. J Cardiovasc Pharmacol 75, 141–147 (2020). [PubMed: 31789884]
62. Tadimalla A, Belmont PJ, Thuerauf DJ, Glassy MS, Martindale JJ, Gude N, Sussman MA, Glembotski CC, Mesencephalic astrocyte-derived neurotrophic factor is an ischemia-inducible secreted endoplasmic reticulum stress response protein in the heart. Circ Res 103, 1249–1258 (2008). [PubMed: 18927462]
63. Matlik K, Anttila JE, Kuan-Yin T, Smolander OP, Pakarinen E, Lehtonen L, Abo-Ramadan U, Lindholm P, Zheng C, Harvey B, Arumae U, Lindahl M, Airavaara M, Poststroke delivery of MANF promotes functional recovery in rats. Sci Adv 4, eaap8957 (2018). [PubMed: 29806020]

64. Tseng KY, Anttila JE, Khodosevich K, Tuominen RK, Lindahl M, Domanskyi A, Airavaara M, MANF Promotes Differentiation and Migration of Neural Progenitor Cells with Potential Neural Regenerative Effects in Stroke. Mol Ther 26, 238–255 (2018). [PubMed: 29050872]

65. Colella P, Ronzitti G, Mingozzi F, Emerging Issues in AAV-Mediated In Vivo Gene Therapy. Mol Ther Methods Clin Dev 8, 87–104 (2018). [PubMed: 29326962]

66. Matlik K, Vihinen H, Bienemann A, Palgi J, Voutilainen MH, Booms S, Lindahl M, Jokitalo E, Saarma M, Huttunen HJ, Airavaara M, Arumae U, Intrastriatally Infused Exogenous CDNF Is Endocytosed and Retrogradely Transported to Substantia Nigra. eNeuro 4, (2017).

67. Reichert K, Colantuono B, McCormack I, Rodrigues F, Pavlov V, Abid MR, Murine Left Anterior Descending (LAD) Coronary Artery Ligation: An Improved and Simplified Model for Myocardial Infarction. J Vis Exp, (2017).

68. Lehmann LH, Cautela J, Palaskas N, Baik AH, Meijers WC, Allenbach Y, Alexandre J, Rassaf T, Muller OJ, Aras M, Asnani AH, Deswal A, Laufer-Perl M, Thuny F, Kerneis M, Hayek SS, Ederhy S, Salem JE, Moslehi JJ, Clinical Strategy for the Diagnosis and Treatment of Immune Checkpoint Inhibitor-Associated Myocarditis: A Narrative Review. JAMA Cardiol 6, 1329–1337 (2021). [PubMed: 34232253]

69. Amancherla K, Qin J, Wang Y, Axelrod ML, Balko JM, Schlendorf KH, Hoffman RD, Xu Y, Lindenfeld J, Moslehi J, RNA-Sequencing Reveals a Distinct Transcriptomic Signature for Giant Cell Myocarditis and Identifies Novel Druggable Targets. Circ Res 129, 451–453 (2021). [PubMed: 34126013]

70. Yang T, Liu YW, Zhao L, Wang H, Yang N, Dai SS, He F, Metabotropic glutamate receptor 5 deficiency inhibits neutrophil infiltration after traumatic brain injury in mice. Sci Rep 7, 9998 (2017). [PubMed: 28855570]

71. Liao Y, Smyth GK, Shi W, featureCounts: an efficient general purpose program for assigning sequence reads to genomic features. Bioinformatics 30, 923–930 (2014). [PubMed: 24227677]

72. Robinson MD, McCarthy DJ, Smyth GK, edgeR: a Bioconductor package for differential expression analysis of digital gene expression data. Bioinformatics 26, 139–140 (2010). [PubMed: 19910308]

73. Yu G, Wang LG, Han Y, He QY, clusterProfiler: an R package for comparing biological themes among gene clusters. OMICS 16, 284–287 (2012). [PubMed: 22455463]

74. Yokota T, McCourt J, Ma F, Ren S, Li S, Kim TH, Kurmangaliyev YZ, Nasiri R, Ahadian S, Nguyen T, Tan XHM, Zhou Y, Wu R, Rodriguez A, Cohn W, Wang Y, Whitelegge J, Ryazantsev S, Khademhosseini A, Teitell MA, Chiou PY, Birk DE, Rowat AC, Crosbie RH, Pellegrini M, Seldin M, Lusis AJ, Deb A, Type V Collagen in Scar Tissue Regulates the Size of Scar after Heart Injury. Cell 182, 545–562 e523 (2020). [PubMed: 32621799]

75. Nelson JD, Denisenko O, Bomsztyk K, Protocol for the fast chromatin immunoprecipitation (ChIP) method. Nat Protoc 1, 179–185 (2006). [PubMed: 17406230]

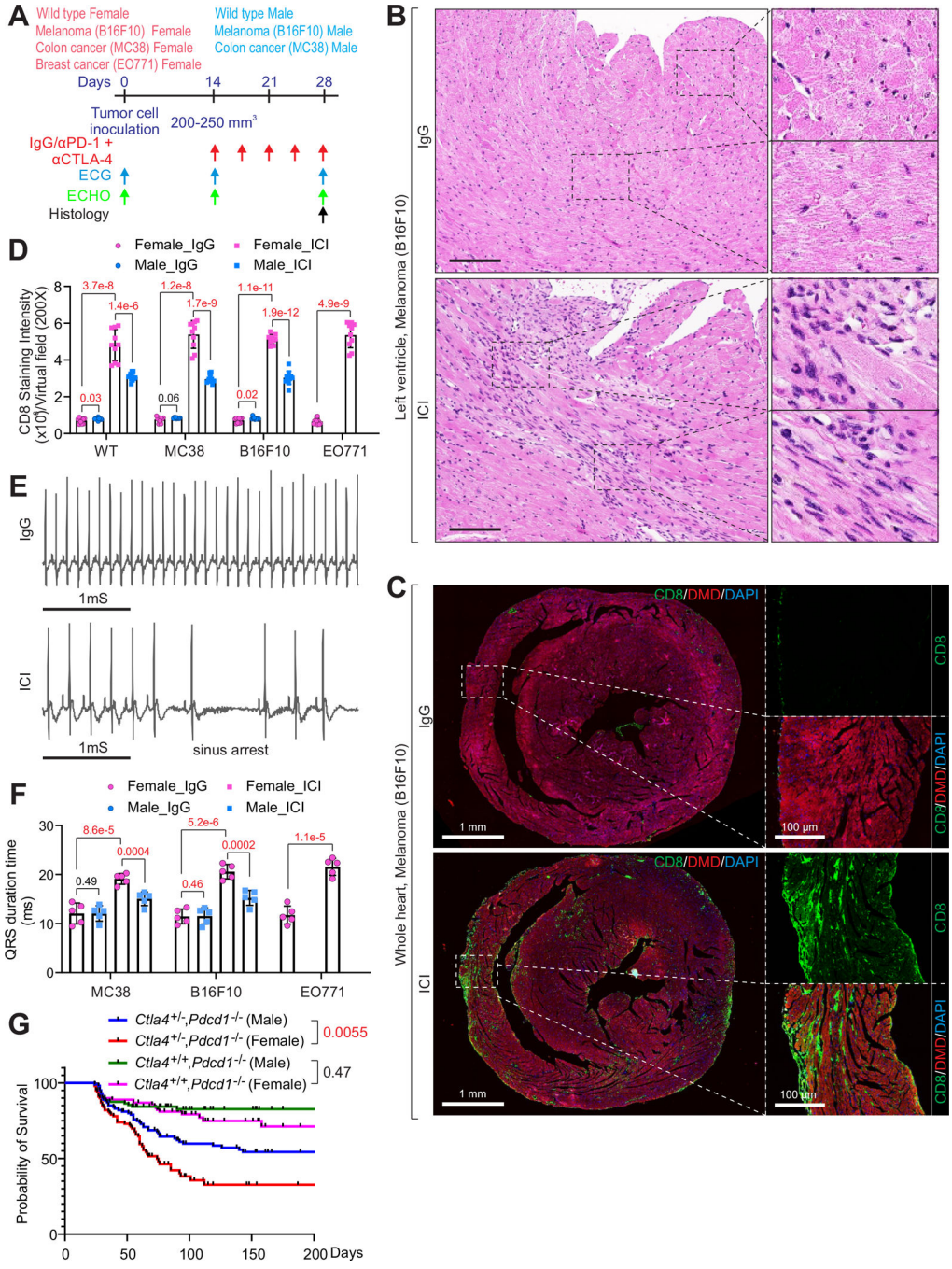

Fig. 1. Characterization of ICI-induced cardiotoxicities in mice.

(**A**) Graphic illustration of experimental setting. (**B**) Representative hematoxylin and eosin (H&E) staining of heart tissues from the female mice inoculated with B16F10 cells, followed by the IgG or ICI treatment. Scale bars, 100 μm. (**C** and **D**) Representative multiplex immunohistochemistry (mIHC) staining using the indicated antibodies (C) and statistical analysis of CD8 staining intensities (D) of heart tissues of the female and male wild type (WT), MC38-, B16F10- or EO771-tumor bearing mice respectively, treated with IgG or ICI (25mg/kg each) (D). Scale bars, 1 mm or 100 μm as indicated. Error bars,

SD, n = 10 animals per experimental group, one-way ANOVA. (**E** and **F**) Representative monitoring lead II ECG traces (E) and statistical analysis of QRS duration (F) from the female mice inoculated with MC38, B16F10 or EO771 cells and treated with IgG or ICI. The implanted monitoring ECG shows sinus arrest in the ICI condition. Error bars, SD, n = 5 animals per experimental group, one-way ANOVA. (**G**) Kaplan-Meier survival curve of *Ctla*4$^{+/-}$/*Pdcd*1$^{-/-}$ and littermate *Ctla*4$^{+/+}$/*Pdcd*1$^{-/-}$ mice (male and female separately, n = 100, 100, 100, 100 animals). *P* value represents the result of the Mantel-Cox log-rank test. n.s.: $P > 0.05$; *$P < 0.05$; **$P < 0.01$; ***$P < 0.001$; ****$P < 0.0001$.

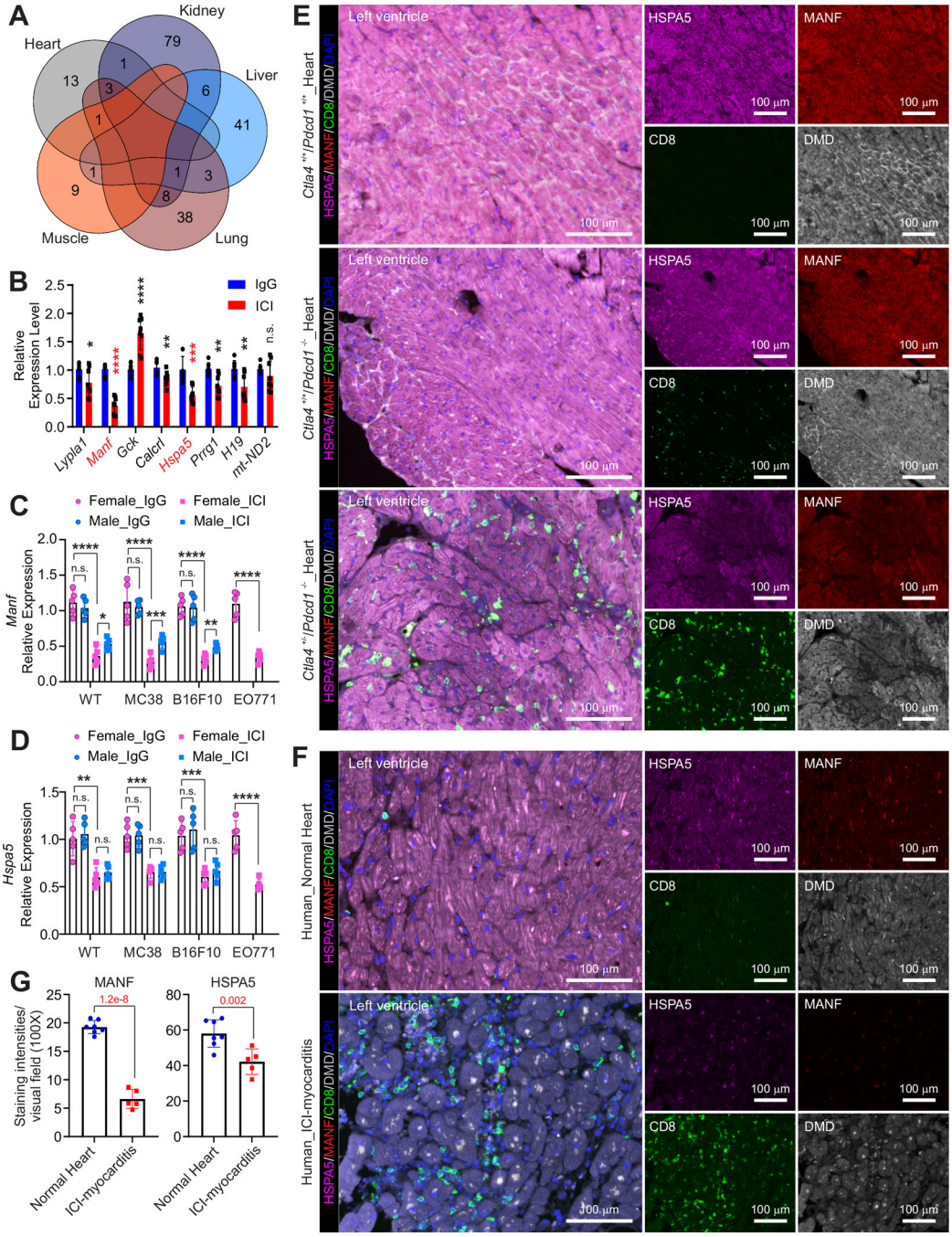

Fig. 2. ICI modulates cardiac expression of MANF and HSPA5 in human and mouse hearts.

(**A**) Venn diagrams present the number of significantly DEGs, which is unique to the specific tissues or shared between tissues (the ICI- versus IgG-treated mouse, see also **GSE145573**). (**B**) RT-qPCR analysis of the indicated genes in heart tissues from female WT, MC38-, B16F10- or EO771 tumor-bearing mice treated with the indicated treatment. Error bars, SD, n = 9 animals per experimental group, Student's *t*-test. (**C** and **D**) Statistical analysis of *Manf* (C) and *Hspa5* (D) gene expression in the hearts of male and female WT, MC38-, B16F10- or EO771 tumor-bearing mice treated with IgG or ICI. Error bars, SD, n = 5

animals per experimental group, Student's *t*-test. **(E)** Representative mIHC staining of heart tissues of female *Ctla*4$^{+/-}$/*Pdcd*1$^{-/-}$ or littermate *Ctla*4$^{+/+}$/*Pdcd*1$^{-/-}$ mice using the indicated antibodies. Scale bars, 100 μm as indicated. (**F** and **G**) Representative mIHC staining images using the indicated antibodies (F) and statistical analysis of MANF and HSPA5 staining intensities (G) of normal human heart tissues or ICI induced myocarditis human heart tissues. Scale bars, 100 μm. Error bars, SD, n = 7, 5 independent visual fields in each experimental group, Student's *t*-test. n.s.: $P > 0.05$; *$P < 0.05$; **$P < 0.01$; ***$P < 0.001$; ****$P < 0.0001$.

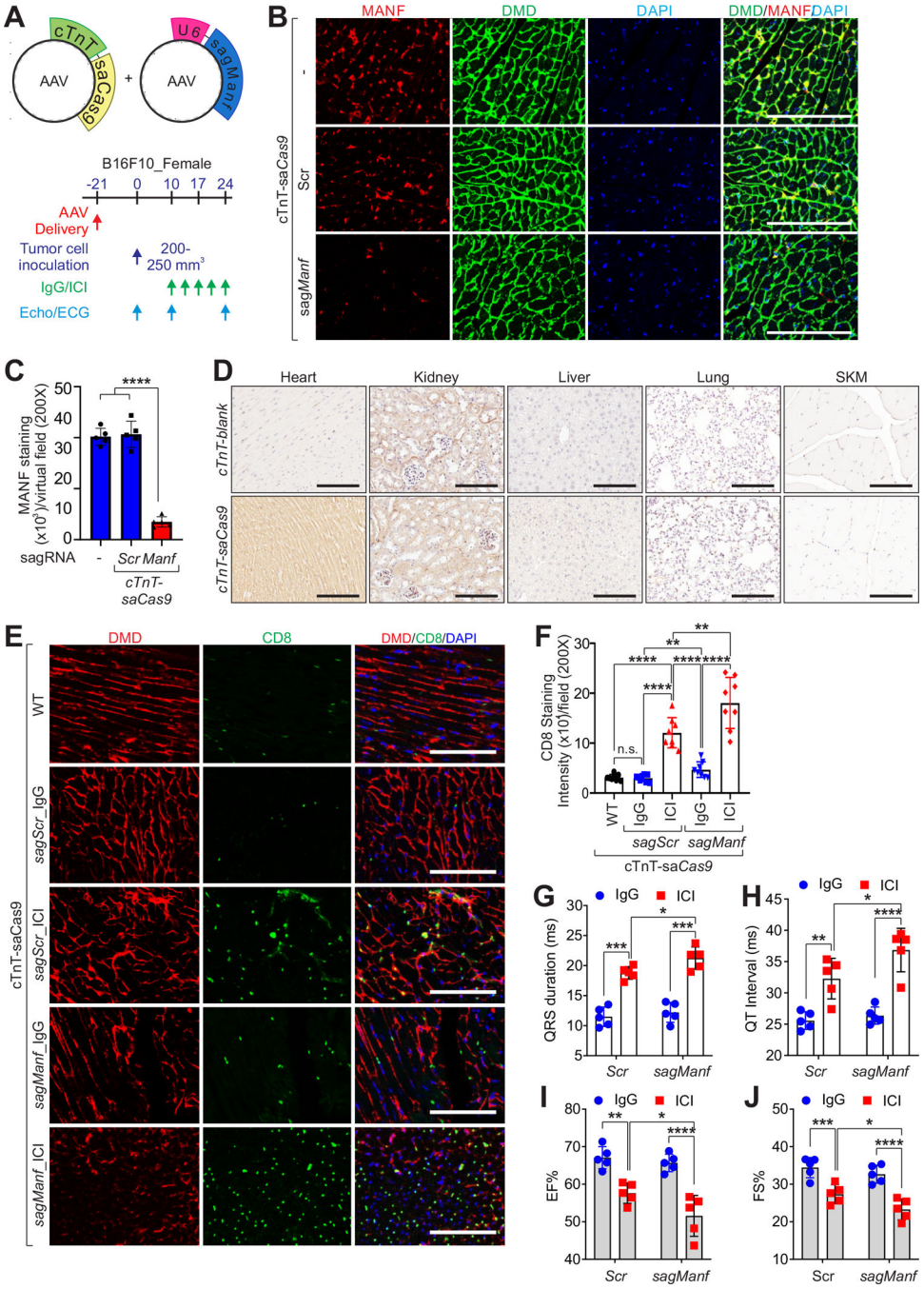

Fig. 3. Deficiency of *Manf* aggravated ICI treatment-induced cardiotoxicities in mice.

(**A**) Graphic illustration of experimental setting. (**B** and **C**) Representative mIHC images using the indicated antibodies (C) and statistical analysis of MANF staining intensities (D) of the hearts administrated with AAV-*cTnT*-s*aCas9* and indicated sagRNAs. Scale bars, 100 μm. Error bars, SD, n = 5 animals per experimental group, One-way ANOVA. (**D**) Representative IHC staining of the indicated mouse tissues upon *cTnT*-blank or -s*aCas9* expression using anti-Cas9 antibody. Scale bars, 100 μm. (**E** and **F**) Representative mIHC images using the indicated antibodies (E) and statistical analysis of CD8 staining intensities

(F) of WT or B16F10 tumor-bearing female hearts administrated with AAV-*cTnT-saCas9* and indicated sagRNAs, followed by the IgG or ICI treatment. Scale bars, 100 μm. Error bars, SD, n = 8 animals per experimental group, one-way ANOVA. WT mice delivered with AAV-cTnT-saCas9 were included as control. (**G** to **J**) Statistical analysis of QRS duration (G), QT interval (H), ejection fraction (%) (I) or fractional shortening (FS%) (J) of WT or tumor-bearing female mice administrated with AAV-*cTnT-saCas9* and indicated sagRNAs, followed by the IgG or ICI treatment. Error bars, SD, n = 5 animals per experimental group, one-way ANOVA. n.s.: $P > 0.05$; *$P < 0.05$; **$P < 0.01$; ***$P < 0.001$; ****$P < 0.0001$.

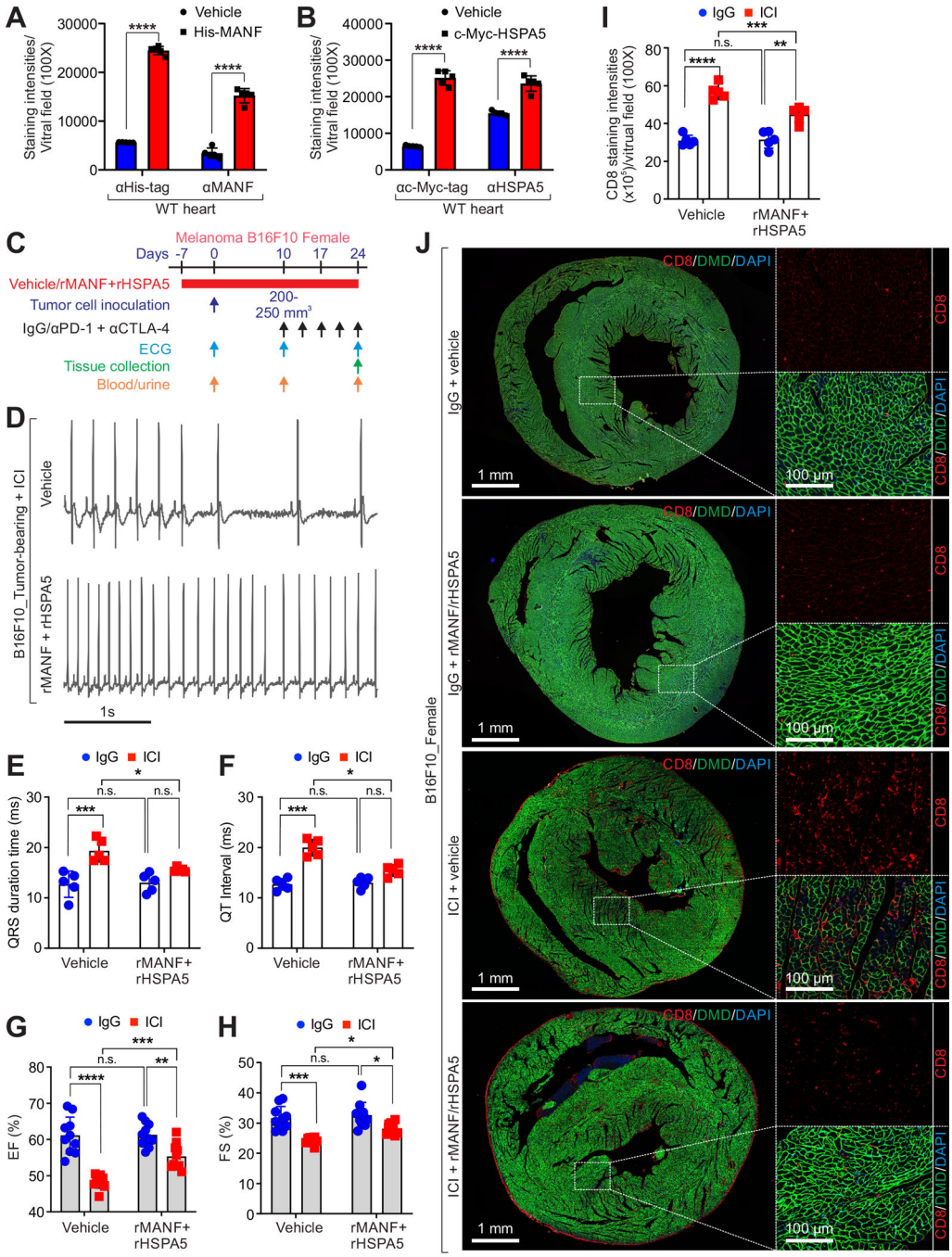

Fig. 4. Recombinant MANF/HSPA5 attenuated ICI-induced cardiotoxicities.

(**A** and **B**) Statistical analysis of staining intensities of His-tag or anti-MANF antibodies (A), anti-c-Myc-tag or anti-HSPA5 antibodies (B) in the heart treated with the vehicle or recombinant MANF+HSPA5 (2 μg/kg and 7.8 μg/kg respectively). Error bars, SD, n = 5 animals per group, Student's *t*-test. (**C**) Graphic illustration of experimental setting. (**D**) Representative monitoring lead II ECG traces from the female B16F10 tumor-bearing mice with the indicated treatment. (**E** and **F**) Statistical analysis of QRS duration (E) or QT interval (F) of monitoring lead II ECG traces from the female B16F10-bearing

mice with the indicated treatment. Error bars, SD, n = 5 animals per experimental group, one-way ANOVA. (**G** and **H**) Statistical analysis of EF% (G) or FS% (H) of the female B16F10 tumor-bearing mice with the indicated treatment. Error bars, SD, n = 5 animals per experimental group, one-way ANOVA. **(I** and **J)** Statistical analysis of CD8 staining intensities (I) and representative mIHC staining (J) of the hearts from the female B16F10 tumor-bearing mice with the indicated treatment. Scale bars, 1mm or 100 μm as indicated. Error bars, SD, n = 5 animals per experimental group, one-way ANOVA. n.s.: $P > 0.05$; *$P < 0.05$; **$P < 0.01$; ***$P < 0.001$; ****$P < 0.0001$.

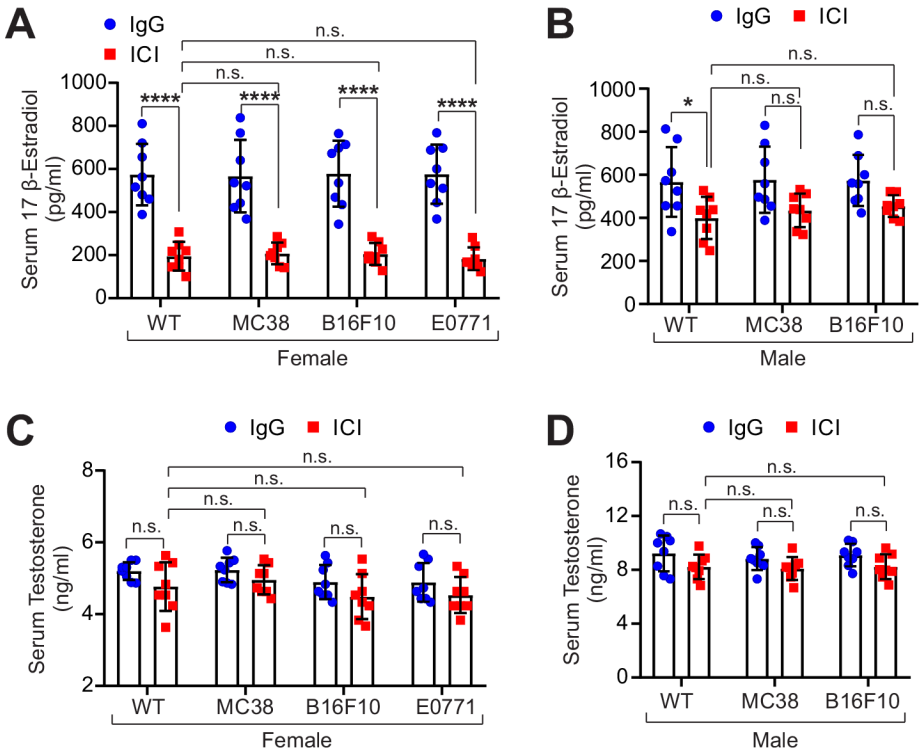

Fig. 5. ICI treatment decreased 17 β-estradiol in mouse serum.

(**A** and **B**) Serum 17 β-estradiol concentration measurement of the female (A) and male (B) WT and tumor-bearing mice that received IgG or ICI treatment. Error bars, SD, n = 8 animals per experimental group, two-way ANOVA. (**C** and **D**) Serum testosterone concentration measurement of the female (C) or male (D) WT or tumor-bearing mice that received IgG or ICI treatment. Error bars, SD, n = 8 animals per experimental group, two-way ANOVA. n.s.: $P > 0.05$; *$P < 0.05$; **$P < 0.01$; ***$P < 0.001$; ****$P < 0.0001$.

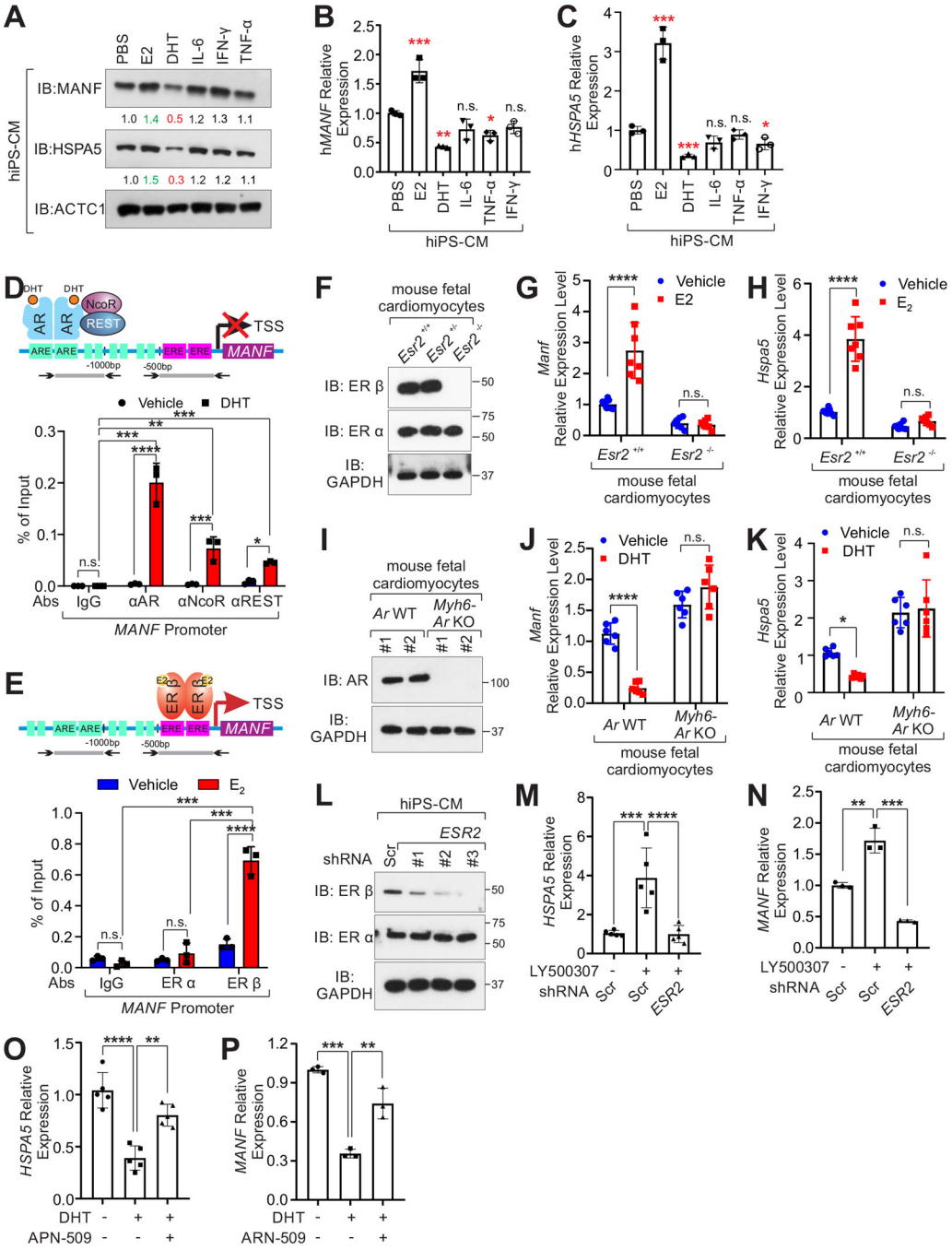

Fig. 6. ICI treatment inhibits estrogen-dependent transcription of *Manf* and *Hspa5*.

(**A**) Immunoblotting (IB) of MANF and HSPA5 in hiPS-CMs with indicated stimulation. ACTC1 was used as a loading control to normalize the relative intensities of MANF and HSPA5 (shown as fold change). (**B** and **C**) RT-qPCR analysis of *MANF* (B) or *HSPA5* (C) mRNA expression in hiPS-CMs following the indicated stimulation. Error bars, SD, n = 3 independent experiments, Student's *t*-test. (**D** and **E**) ChIP-qPCR analysis of the occupancy of indicated proteins on *MANF* promoter in hiPS-CMs after the indicated stimulation. Error bars, SD, n = 3 independent experiments, one-way ANOVA. (**F**) IB of ERβ and ERα in

Esr2$^{+/+}$ or *Esr2*$^{-/-}$ mouse fetal cardiomyocytes. GAPDH was used as a loading control. (**G** and **H**) RT-qPCR analysis of *Manf* (G) or *Hspa5* (H) mRNA expression in *Esr2*$^{+/+}$ or *Esr2*$^{-/-}$ mouse fetal cardiomyocytes with indicated stimulation. Error bars, SD, n = 7 animals per experimental group, Student's *t*-test. (**I**) IB of AR in *Ar*-proficient or *Myh6-Ar* knockout mouse fetal cardiomyocytes with indicated stimulation. (**J** and **K**) RT-qPCR analysis of *Manf* (J) or *Hspa5* (K) mRNA expression in *Ar*-proficient or *Myh6-Ar* knockout mouse fetal cardiomyocytes with indicated stimulation. Error bars, SD, n = 6 animals per experimental group, Student's *t*-test. (**L**) IB of the indicated proteins in hiPS-CMs harboring indicated shRNAs. (**M** to **N**) RT-qPCR analysis of *HSPA5* (M) or *MANF* (N) mRNA expression in hiPS-CMs harboring indicated shRNAs, that received indicated treatments. Error bars, SD, n = 5 independent experiments, one-way ANOVA. (**O** to **P**) RT-qPCR detection of *HSPA5* (O) or *MANF* (P) in hiPS-CMs treated with indicated stimuli. Error bars, SD, n = 3 independent experiments, one-way ANOVA. n.s.: $P > 0.05$; *$P < 0.05$; **$P < 0.01$; ***$P < 0.001$; ****$P < 0.0001$.

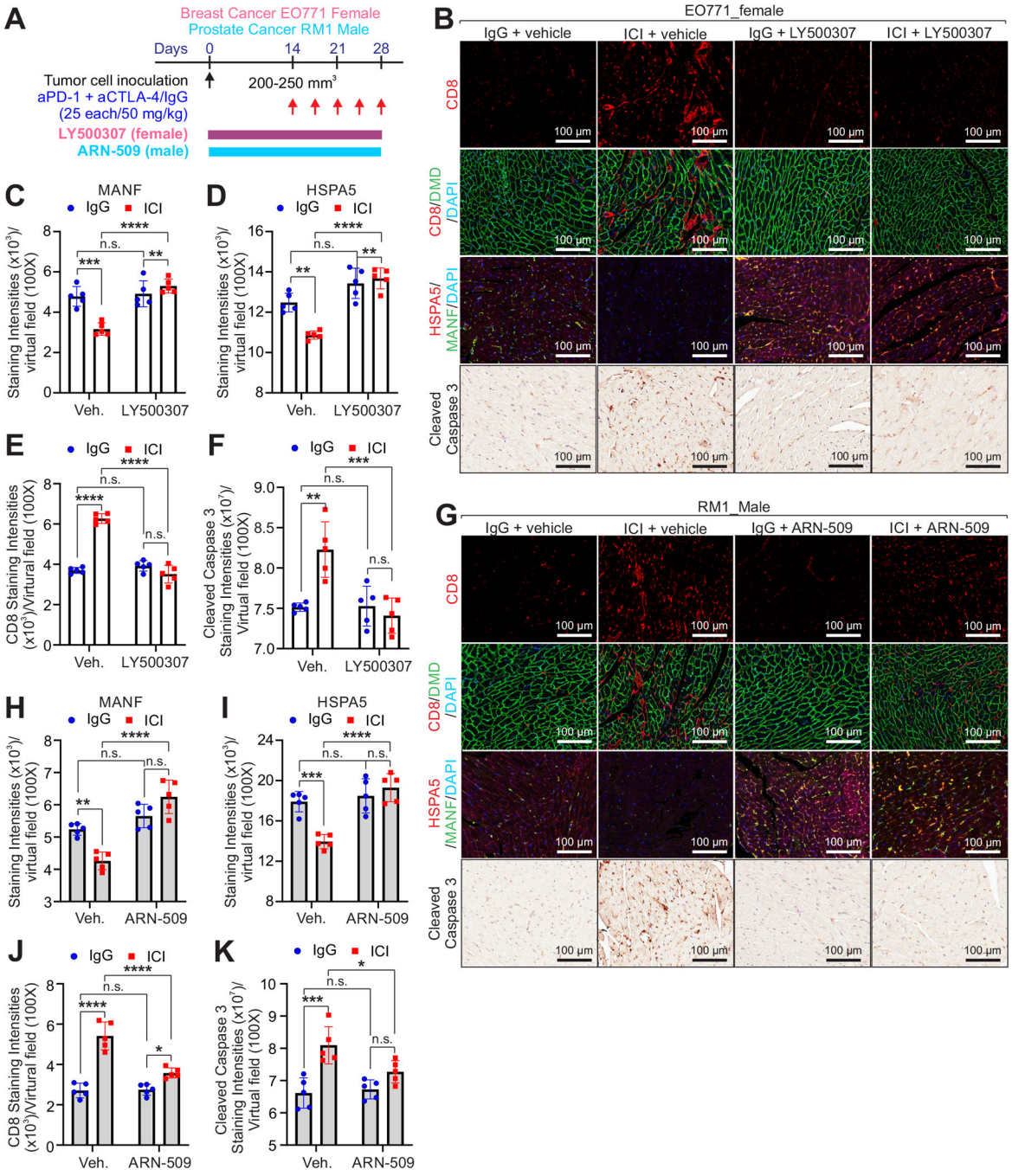

Fig. 7. Hormone therapy minimized ICI-induced cardiotoxicities in mice.

(**A**) Graphic illustration of experimental setting. (**B** to **F**) Representative mIHC and IHC staining images using the indicated antibodies (B), and staining intensity statistical analysis of MANF (C), HSPA5 (D), CD8 (E) or cleaved caspase 3 (F) in the hearts of EO771 tumor-bearing female mice that received indicated treatments. Scale bars (B), 100 μm. Error bars (C-F), SD, n = 5 animals per experimental group, one-way ANOVA. (**G** to **K**) Representative mIHC and IHC staining using the indicated antibodies (G), and staining intensity statistical analysis of MANF (H), HSPA5 (I), CD8 (J) or cleaved caspase 3 (K) in

the hearts of RM1 tumor-bearing male mice that received the indicted treatments. For C to F and H to K, blue dot and red square represents IgG and ICI treatment respectively in both vehicle and LY500307 or ARN-509 groups. Scale bars (G), 100 μm. Error bars (H-K), SD, n = 5 animals per experimental group, one-way ANOVA. n.s.: $P > 0.05$; *$P < 0.05$; **$P < 0.01$; ***$P < 0.001$; ****$P < 0.0001$.